Journal of
Medicinal Chemistry

Article

Discovery of a New Isoxazole-3-hydroxamate Based Histone Deacetylase 6 Inhibitor SS-208 with Anti-tumor Activity in Syngeneic Melanoma Mouse Models

Sida Shen, Melissa Hadley, Kseniya Ustinova, Ji#í Pavlí#ek, Tessa Knox, Satish Noonepalle, Mauricio Temotheo Tavares, Chad A. Zimprich, GuiPing Zhang, Matthew B. Robers, Cyril Barinka, ALAN KOZIKOWSKI, and Alejandro Villagra

J. Med. Chem., **Just Accepted Manuscript** • DOI: 10.1021/acs.jmedchem.9b00946 • Publication Date (Web): 15 Aug 2019

Just Accepted

is published by the American Chemical Society. 1155 Sixteenth Street N.W., Washington, DC 20036

Discovery of a New Isoxazole-3-hydroxamate Based Histone Deacetylase 6 Inhibitor SS-208 with Anti-tumor Activity in Syngeneic Melanoma Mouse Models

Sida Shen[3,‡,†], Melissa Hadley[1,‡], Kseniya Ustinova[4], Jiri Pavlicek[4], Tessa Knox[1], Satish Noonepalle[1], Mauricio T. Tavares[3,□], Chad A. Zimprich[5], Guiping Zhang[6], Matthew B. Robers[5], Cyril Bařinka[4], Alan P. Kozikowski[,2], Alejandro Villagra*[,1]*

[1] Department of Biochemistry and Molecular Medicine, The George Washington University, Washington, District of Columbia 20052, United States.

[2] StarWise Therapeutics LLC, University Research Park, Inc., Madison, Wisconsin 53719, United States.

[3] Department of Medicinal Chemistry and Pharmacognosy, College of Pharmacy, University of Illinois at Chicago, Chicago, Illinois 60612, United States.

[4] Laboratory of Structural Biology, Institute of Biotechnology of the Czech Academy of Sciences, Prumyslova 595, 252 50 Vestec, Czech Republic.

[5] Promega Corporation, Madison, Wisconsin 53711, United States.

[6] Bontac Bio-Engineering (Shenzhen) Co., Ltd, Shenzhen, Guangdong 518102, China.

KEYWORDS: Ames-negative, catalytic domain 2, acetylated α-tubulin, non-cytotoxic, immunoregulation

ABSTRACT

Isoxazole is a five-membered heterocycle that is widely used in drug discovery endeavors. Here, we report the design, synthesis, and structural and biological characterization of SS-208, a novel HDAC6-selective inhibitor containing the isoxazole-3-hydroxamate moiety as a zinc-binding group as well as a hydrophobic linker. A crystal structure of the *Danio rerio* HDAC6/SS-208 complex reveals a bidentate coordination of the active-site zinc ion that differs from the preferred monodentate coordination observed for HDAC6 complexes with phenylhydroxamate-based inhibitors. While SS-208 has minimal effects on the viability of murine SM1 melanoma cells *in vitro*, it significantly reduced *in vivo* tumor growth in a murine SM1 syngeneic melanoma mouse model. These findings suggest the antitumor activity of SS-208 is mainly mediated by immune-related antitumor activity as evidenced by the increased infiltration of CD8+ and NK+ T cells and the enhanced ratio of M1 and M2 macrophages in the tumor microenvironment.

INTRODUCTION

Malignant melanoma represents the most aggressive and the deadliest form of cutaneous cancer with increasing incidence, high metastasis, rapid disease progression, poor prognosis, and high mortality.[1, 2] Patients with metastatic melanoma have poor prognosis with a 5-year survival rate of less than 10%.[3] A few targeted agent therapies have recently become available for metastatic melanoma. For instance, BRAF inhibitors (i.e., dabrafenib) and MEK1/2 inhibitors (trametinib) have been approved as monotherapy or combined approach for the treatment of melanoma with mutation.[4] However, the clinical benefit of these therapies is limited due to the rapid development of resistance associated with the activation of alternative pro-oncogenic pathways.[4] Within the last five years, immunotherapy has revolutionized the treatment of patients with advanced-stage melanoma. Antibodies that block the negative co-stimulatory receptors CTLA-4 (ipilimumab)[5, 6], and PD-1 (nivolumab and pembrolizumab)[7-9] have been approved based on significantly longer overall survival in clinical trials compared to other therapies. The objective response rates of these immune checkpoint blockades are around 20-30%,[10] while primary, adaptive, and acquired resistance to immunotherapy is common and may be related to the lack of recognition by T-cells.[11, 12] Novel aiming to overcome these limitations, especially on the resistance mechanisms originated in other components of the tumor microenvironment (TME) are still highly needed to improve currently available therapeutics.[13-16]

Histone deacetylases (HDACs) are a family of proteins involved in the epigenetic regulation of target genes through deacetylating lysine ε-amino groups on histone tails to promote a status of DNA condensation and transcriptional silencing.[17] Furthermore,

HDACs have been found to modify other non-histone proteins, and these modifications can influence a variety of cellular functions without modifying the acetylation of the chromatin acetylation status.[18-20] HDACs have been proven to be promising therapeutic targets for the treatment of cancer based on the successful launch of five HDAC inhibitors (vorinostat, romidepsin, panobinostat, belinostat, and chidamide) which are relatively non-selective.[21, 22] In general, broad-spectrum HDAC inhibitors (pan-HDACis) are involved in chromosome remodeling, cell cycle arrest, apoptosis, and cytotoxicity in transformed cancer cells.[23, 24] In addition to these effects, there is growing evidence to demonstrate that the treatment with HDACis increases differentiation antigen expression, enhances MHC class I and II surface expression, and elevates immunogenicity in terms of increased expression of CD25, CD40, or CD80.[25, 26] It has been reported that pan-HDACis can upregulate the expression of PD-L1 and PD-L2 in human and murine melanoma cells.[27] Therefore, pan-HDACis show ability to possess anti-tumor activity through inhibiting proliferation and improving immune responses.[28] However, phase I/II clinical trials of pan-HDACis (vorinostat, panobinostat, and quisinostat) with melanoma patients only exhibited limited efficacy and tolerability as single agents, while hematological toxicity, fatigue, nausea, and laboratory abnormalities occurred as frequent adverse events.[26] Important concerns regarding the toxicity of pan-HDACis are rising since their broad inhibition may result in unwanted off-target effects that eventually impair their clinical profile. Thus, there is an emerging interest in the development and investigation of selective HDACis to better understand the molecular mechanisms mediating the anti-tumor effects.[29] So far, there are few subtype-selective or isoform-selective inhibitors that are non-cytotoxic and better tolerated, and that effectively impair tumor growth in preclinical models.[30-35]

Eighteen known mammalian HDACs have been identified, which can be classified into four subgroups according to their homology to yeast enzymes: class I (HDAC1, 2, 3, and 8), class IIa (HDAC4, 5, 7, and 9), class IIb (HDAC6 and HDAC10), class III or sirtuins (SIRT 1−7), and class IV (HDAC11).[36] Class I, II, and IV HDACs require Zn^{2+} (zinc ion) as a cofactor to exert their hydrolytic activity and are also referred to as the conventional HDACs. On the other hand, SIRT 1−7 are dependent on nicotinamide adenine dinucleotide for their activity.[37] In comparison with other HDAC family members, HDAC6 is relatively unique. It contains two tandem deacetylase catalytic domains (CD1 and CD2) and is primarily localized to the cytosol, and its preferred substrates include a variety of non-histone proteins, such as α-tubulin, cortactin, HSP-90, and HSF-1.[38, 39] Moreover, only CD2 exhibits catalytic activity with broad specificity.[40] Intriguingly, according to a patent survey based on the recent efforts on the synthesis and applications of HDACis from 2013 to 2017, most patents focused on the discovery of new HDAC6 inhibitors (HDAC6is).[41] Up to date, two partially selective HDAC6is, ricolinostat (ACY-1215)[42] and citarinostat (ACY-241),[43] have been advanced into clinical trials for different types of cancer, such as multiple myeloma, lymphoma, breast cancer, and melanoma, through monotherapy or a combination approach. Moreover, selective HDAC6is have been considered as potential therapeutic agents for the treatment of various neurological disorders.[44-46]

HDAC6 promotes the proliferation and metastasis of melanoma cells, and knockdown of HDAC6 decreases proliferation and induces G1 cell cycle arrest of melanoma cells.[28, 47] Moreover, it was found that HDAC6 increases the protein level of tyrosine-protein phosphatase non-receptor type 1 (PTPN1), which is responsible for promoting proliferation, colony formation, and migration while decreasing apoptosis of melanoma

cells through activating extracellular signal-regulated kinase 1/2 (ERK1/2).[48] A preclinical study of ricolinostat showed that this partially selective HDAC6i impaired proliferation and induced apoptosis of BRAF-mutant melanoma A375 cells.[49] Notably, the combination treatment of BRAF inhibitor vemurafenib and ricolinostat displayed a synergetic effect in BRAF-mutant melanoma cells partially through induction of endoplasmic reticulum stress and inactivation of ERK.[49] In addition to the effects on survival, we have found that HDAC6 is a modulator of the expression of specific tumor-associated antigens, MHC class I, and costimulatory molecules in melanoma.[28] In previous works, we reported that either selective pharmacological inhibition or genetic abrogation of HDAC6 plays a critical role in the immune checkpoint blockade by down-regulating the expression of PD-L1, which exhibits an opposite effect relative to class I and pan-HDACis.[50] Also, we recently found that the combination of a selective HDAC6i, nexturastat A (NextA), and PD-1 immune blockade resulted in a significant improvement in anti-tumor immune responses leading to further reduction of tumor growth compared to monotherapy.[51] Taken together, all the preclinical and clinical stage studies indicate that HDAC6 inhibition shows potential to become a promising approach for melanoma therapy. However, neither ricolinostat nor citarinostat can be considered to be highly selective HDAC6is due to their only about 10-fold enzymic selectivity against the class I isoform, HDAC1 (Figure 1).[52, 53] Therefore, there is a need for the advancement of drug candidates with higher selectivity and good pharmacologic attributes.

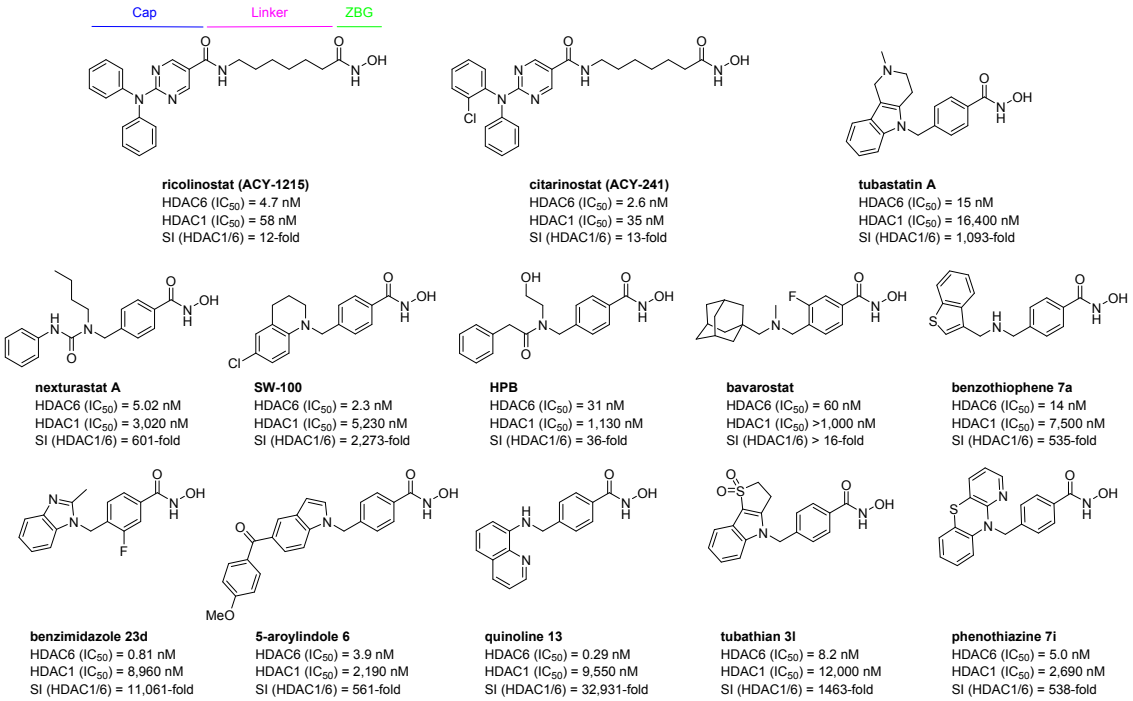

Figure 1. The structures of recent published HDAC6 inhibitors.

A typical HDACi structure contains a zinc-binding group (ZBG) that coordinates the active-site Zn^{2+} at the deep bottom of the substrate pocket, a linker to occupy the hydrophobic channel, and a capping group (cap) to interact with residues at the rim of the catalytic cavity. Recent results suggest that the connecting unit (CU) region that links the cap with the linker and ZBG may strongly impact the ligand's selectivity towards HDAC6.[54] The phenylhydroxamate moiety has been recognized as a useful ZBG as well as a hydrophobic linker in the discovery of selective HDAC6is (Figure 1).[31, 34, 55-64] The majority of recent advancements has concentrated on the development of hydroxamate analogs bearing a phenyl or pyrimidyl ring.[65, 66] Meanwhile, minimal effort has gone into developing linkers containing five-membered heteroaromatics such as thiazole and oxazole.[67, 68] Isoxazole is a five-membered heterocycle which contains two heteroatoms,

one oxygen and one nitrogen atom, in adjacent positions. Two double bonds contribute to the unsaturated character of the molecule. The structural features of isoxazole make it suitable for multiple non-covalent interactions, including hydrogen bonding (N and O as acceptors) and π-π stacking.[69] We note that the isoxazole moiety is a central part of multiple compounds aimed at a wide spectrum of biological targets, and the inclusion of isoxazole in a structure may contribute to its increased efficacy, decreased toxicity, and improved pharmacokinetic profile.[70] Herein, we report on the discovery of SS-208, a novel isoxazole-3-hydroxamate-based, selective HDAC6i, its structural characterization in a complex with the catalytic domain 2 of *Danio rerio* HDAC6 (drHDAC6), and *in vivo* efficacy results in a syngeneic mouse model of melanoma.

RESULTS AND DISCUSSION

Chemistry. In our prior work, we identified an isoxazole-3-hydroxamate-based hit **1a**, which demonstrates potent HDAC6 inhibitory activity and modest potency against HDAC1, a member of class I HDACs,[71] unlike its corresponding alkylhydroxamate (**1b)** and phenylhydroxamate (**1c**) analogs. Moreover, the compound **1d** incorporating the reverse direction of the amide CU dramatically loses selectivity (Figure 2).[71-73] However, the non-ideal physicochemical properties of **1a** (TPSA = 168.82, MW = 457.44, calculated by SwissADME[74]) and short half-lives ($t_{1/2}$) in microsomal stability studies (mouse: 16 min; human: 85 min, determined by Pharmaron, Inc., Irvine, CA) constitute an obstacle for its advance into *in vivo* studies. Notably, **1a** was incubated with two strains of *Salmonella typhimurium* (TA97A and TA1537) by Pharmaron in the presence and absence of mammalian microsomal enzymes (S9 mix) to evaluate the mutagenicity potential of the

hydroxamate moiety.[75] The results in Table S1 indicate that **1a** is Ames-negative under the testing conditions, which encouraged us to pursue further structural tuning in order to discover more druggable isoxazole-3-hydroxamate-based HDAC6is.

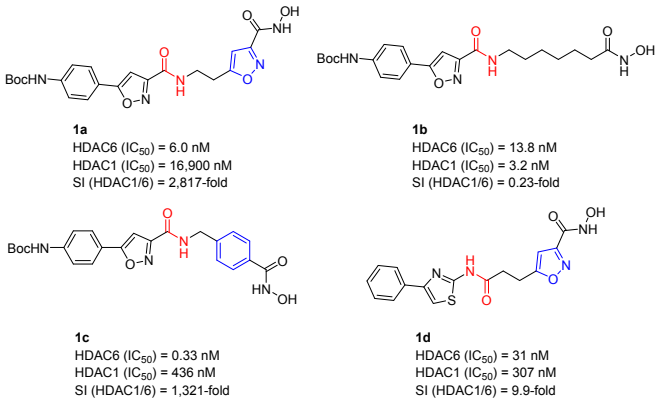

Figure 2. The structures of isoxazole-3-hydroxamate HDAC inhibitors **1a-d**.

To improve the physicochemical properties of this series of compounds, we started our optimization by replacing the Boc-protected phenylisoxazole cap with simple monocyclic and bicyclic aromatic rings (**7a-d**), while keeping the same ethylamide and isoxazole-3-hydroxamate moieties to maintain close structural similarity to **1a**. The synthetic routes to analogs **7a-d** shown in Scheme 1 started from 3-butyn-1-ol (**2a**) and led to the preparation of the same 1-amino-3-butyne intermediate **4** through a Mitsunobu reaction using phthalimide/Ph_3P/DEAD. Subsequent deprotection and acylation with the appropriate acyl chlorides provided the alkyne intermediates **5a-d**. The acetylenic moieties in **5a-d** were transformed into the isoxazole esters **6a-d** by 1,3-dipolar cycloaddition with a nitrile oxide generated in situ from ethyl 2-chloro-2(hydroximino)acetate and a base under microwave conditions.[76] These esters upon treatment with an aqueous NH_2OH/NaOH solution efficiently afforded the desired hydroxamic acids **7a-d** bearing aromatic caps.

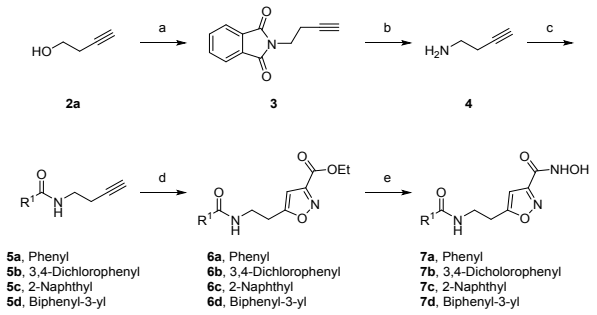

Scheme 1. The synthetic route to compounds **7a-d**. (a) phthalimide, Ph_3P, DEAD, THF, 0 °C to rt, yield: 93%; (b) hydrazine monohydrate, MeOH, rt; (c) ArCOCl, TEA, DCM, 0 °C, yields: 52-90% over two steps; (d) ethyl 2-chloro-2-(hydroxyimino)acetate, $NaHCO_3$, EtOAc, 100 °C (MW), yields: 49-78%; (e) NH_2OH (aq., 50%), NaOH, THF/MeOH (1:1), 0 °C to rt, yields: 10-43%.

Given the wide rim of the HDAC6 substrate pocket, aryl caps bearing a sterically bulky moiety are usually preferred to enhance inhibitor affinity and specificity *via* interactions with the residues forming the surface.[55, 64, 77, 78] Therefore, we further investigated the replacement of the cap and amide CU in **1a** with bicyclic and tricyclic caps. To prepare the indole-capped analogue **11a** illustrated in Scheme 2, 1,3-dipolar cycloaddition of 5-hexyn-1-ol (**2b**) and ethyl 2-chloro-2(hydroximino)acetate was conducted to establish the key isoxazole ester **8a** from the beginning. Subsequently, **8a** underwent bromination with CBr_4/Ph_3P, N-alkylation under Cs_2CO_3/DMF conditions, and transformation to the desired hydroxamate analog **11a** in the presence of an aqueous NH_2OH/NaOH solution. The synthetic routes to **11b-c** started from 4-chloroaniline (**12**), which was first converted to the *N*-phenyl amides **13a-b** by treating with 3-chloropropanoyl chloride and 3,3-dimethylacryloyl chloride, respectively. Subsequently, intramolecular Friedel–Crafts cyclization under $AlCl_3$ conditions followed by reduction of the intermediate lactam with

$LiAlH_4$ afforded the tetrahydroquinolines **14a-b**.[63, 79] Reductive amination of **14a-b** and the aldehyde intermediate **9b** which was prepared from **8a** by PCC oxidation, provided the corresponding esters **10b-c**. In the end, the desired hydroxamate analogs **11b-c** were obtained using the same standard procedure as above. The synthetic route to the dibenz[*b,f*]azepine-capped analog **11d** began with the dichlorination of **15** using NCS/silica gel[80] followed by *N*-alkylation with 1,4-dibromobutane under NaH/DMF conditions and alkynation with sodium acetylide to provide the key dibenz[*b,f*]azepine-substituted alkyne **18**. Then the building block **18** underwent 1,3-dipolar cycloaddition, and the desired isoxazole-3-hydroxamate **11d** was then obtained in the usual manner.

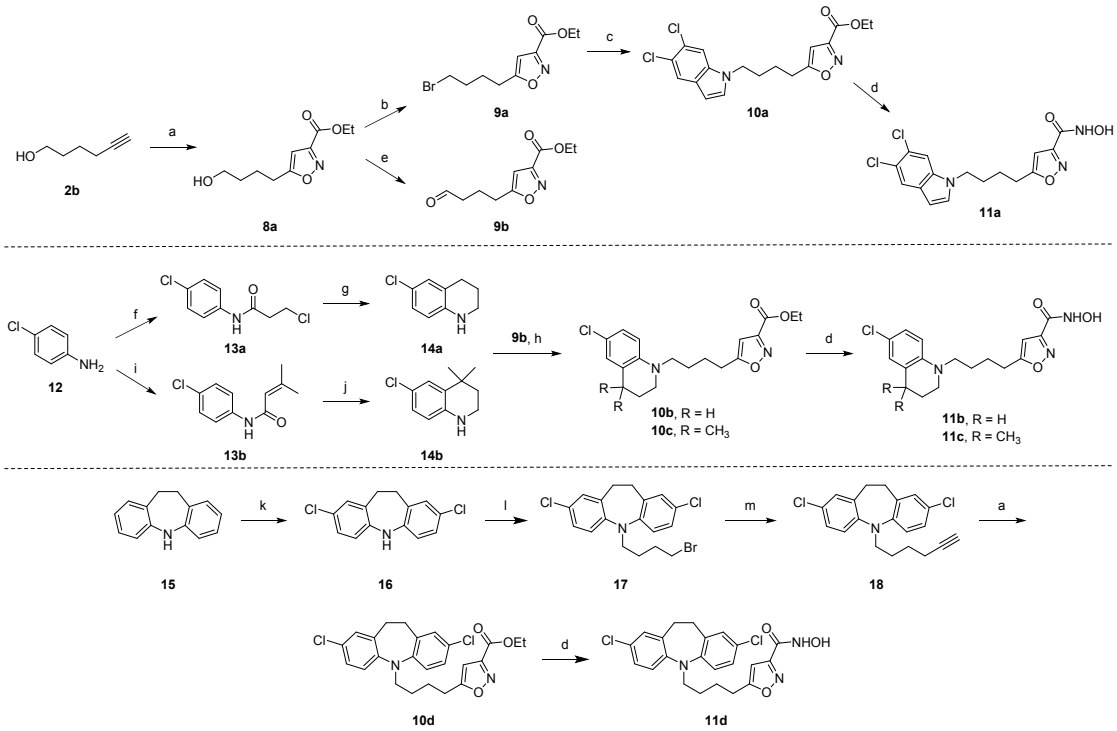

Scheme 2. The synthetic routes to compounds **11a-d**. (a) ethyl 2-chloro-2-(hydroxyimino)acetate, $NaHCO_3$, EtOAc, 100 °C (MW), yields: 67-87%; (b) CBr_4, Ph_3P, DCM, rt, yield: 89%; (c) 5,6-dichloro-1*H*-indole, Cs_2CO_3, DMF, 80 °C, 80%; (d) NH_2OH (aq., 50%), NaOH, THF/MeOH (1:1), 0 °C to rt, yields: 34-94%; (e) PCC, DCM, rt, yield:

88%; (f) 3-chloropropanoyl chloride, acetone, reflux, yield: 54%; (g) i) $AlCl_3$, 140 °C (neat), ii) $LiAlH_4$, THF, 0 °C to reflux, yield: 70% over two steps; (h) **9b**, $NaBH(OAc)_3$, AcOH/EtOH, rt, yields: 42-58%; (i) 3,3-dimethylacryloyl chloride, $CHCl_3$, reflux, yield: 48%; (j) i) $AlCl_3$, toluene, 80 °C, ii) $LiAlH_4$, THF, 0 °C to reflux, yield: 55% over two steps; (k) NCS, silica gel, $CHCl_3$, rt, yield: 74%; (l) 1,4-dibromobutane, NaH, DMF, rt, yield: 43%; (m) sodium acetylide, xylene/DMF, 40 °C, yield: 25%.

As a 3,4-dichlorophenyl cap on **7b** retained HDAC6 potency and selectivity over HDAC1 (data are shown in Table 1), we further synthesized compounds **20a-c** in order to evaluate the effects of the amide CU and isoxazole-based ZBG. To prepare the analog **20a** which contains an ether linker in place of the amide group, the synthetic route shown in Scheme 3 was followed. 1,3-Dipolar cycloaddition between 4-pentyn-1-ol (**2c**) and ethyl 2-chloro-2-(hydroximino)acetate generated the isoxazole ring (compound **8b**). This intermediate underwent bromination with CBr_4/Ph_3P followed by O-alkylation with 3,4-dichlorophenol under Cs_2CO_3/DMF conditions. The synthesis was completed as above to afford the desired hydroxamate **20a**. To synthesize analog **20b** which only contains an alkyl chain rather than an amide group, the α,β-unsaturated carboxylic acid in the starting material **21** was first transformed to a bromoalkyl intermediate **22** through $LiAlH_4$ reduction and bromination with CBr_4/Ph_3P. Compound **22** was further converted to the nitrile **23** with NaCN. Subsequent hydrolysis under basic condition and borane reduction provided the butanol **24**. The alkyne **25** was obtained through bromination and alkynation under similar conditions as described above and underwent 1,3-dipolar cycloaddition and conversion to the hydroxamic acid **20b**. The synthetic route to the benzyl hydroxamate analog **20c** started

from $Cu(OAc)_2$-catalyzed one-pot conversion of 3,4-dichlorobenzaldehyde (**26**) into 3,4-dichlorobenzamide (**27**) through a Beckmann-type rearrangement.[81] Subsequent reductive N-alkylation of the amide intermediate **27** using TFA/Et_3SiH with methyl 4-formylbenzoate led to the generation of the corresponding ester **19c**,[82] which upon standard treatment afforded the desired hydroxamate **20c**.

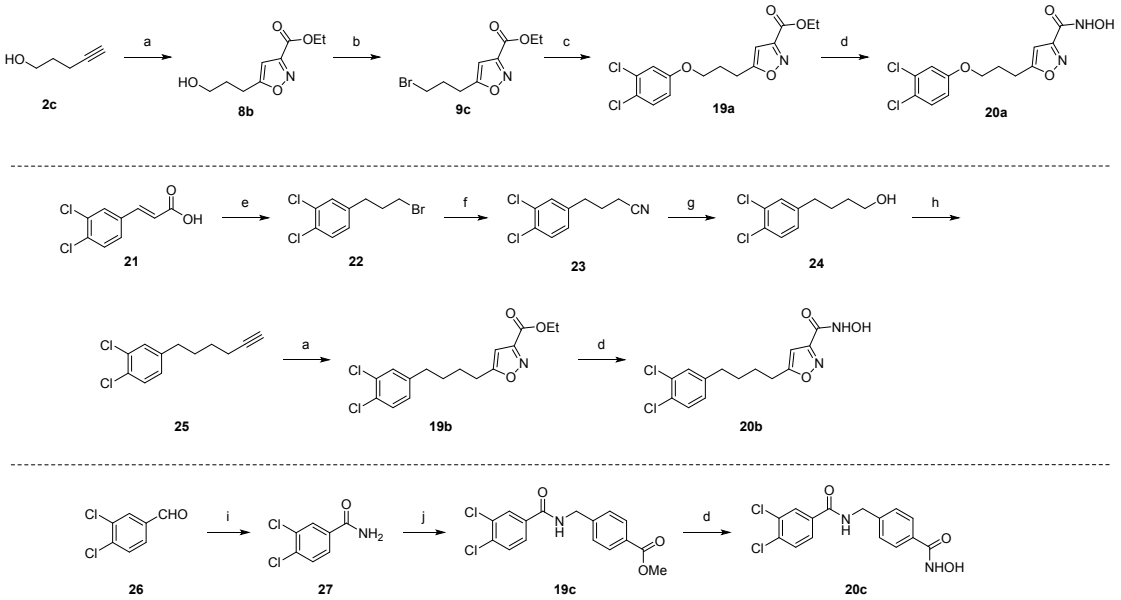

Scheme 3. The synthetic routes to compounds **20a-c**. (a) ethyl 2-chloro-2-(hydroxyimino)acetate, $NaHCO_3$, EtOAc, 100 °C (MW), yields: 58%-96%; (b) CBr_4, Ph_3P, DCM, rt, yield: 83%; (c) 3,4-dichlorophenol, Cs_2CO_3, DMF, 80 °C, yield: 80%; (d) NH_2OH (aq., 50%), NaOH, THF/MeOH (1:1), 0 °C to rt, yields: 30-40%; for **20c**, yield: 22% over three steps; (e) i) $LiAlH_4$, THF, 0 °C to reflux, ii) CBr_4, Ph_3P, DCM, 0 °C to rt, yield: 11% over two steps; (f) NaCN, DMSO, 100 °C, yield: 72%; (g) i) aq. NaOH, EtOH, reflux, ii) BH_3-THF, THF, 0 °C to rt, yield: 88% over two steps; (h) i) CBr_4, Ph_3P, DCM, rt, ii) sodium acetylide, DMF, 40 °C, yield: 39% over two steps; (i) $NH_2OH{\cdot}HCl$, K_2CO_3, $Cu(OAc)_2$, H_2O, reflux; (j) TFA, Et_3SiH, methyl 4-formylbenzoate, toluene, reflux.

HDAC Isoform Inhibition. To evaluate isoform potency and selectivity of all new analogs (**7a-d**, **11a-d**, and **20a-c**), we first prescreened their inhibitory activity against human HDAC6 and HDAC1 *in vitro* (performed by Reaction Biology Corp, Malvern, PA). As illustrated in Table 1, the replacement of the phenylisoxazole cap of the parent compound **1a** with phenyl rings as in compounds **7a-b** led to a 12.5-fold to 32-fold decrease in inhibitory potency for HDAC6, while micromolar inhibition values against HDAC1 remained constant. Compounds **7c-d,** in which the cap moiety was replaced with a naphthyl or biphenyl group, retained low nanomolar inhibitory potency for HDAC6 with a concomitant decrease of the HDAC1/HDAC6 selectivity index. Notably, this replacement significantly decreased the number of heavy atoms and TPSA values compared to the hit **1a** (Table S2) and improved the ligand efficiency (LE) values beyond 0.4 while keeping the lipophilic ligand efficiency (LipE) values above 5.0 (Table 1).[83, 84] Incorporation of sterically bulky caps into the molecule to form the bicyclic- or tricyclic-capped analogs **11a-d** resulted in a significant decrease in potency, and none of them delivered meaningful ligand efficiency values (LE and LipE). Replacement of the amide moiety in **7b** with an ether (**20a**) or alkyl chain (**20b**) was also disadvantageous, as it resulted in a 3-fold to 26-fold decrease in HDAC6 potency, suggesting that the amide moiety is necessary for retaining high potency in this class. Compared to **7b**, its corresponding phenylhydroxamate analog **20c** demonstrated about 3-fold improvement in HDAC6 potency (IC_{50} = 28 nM) and similar ligand efficiency values. However, the isozyme selectivity significantly fell to around 7-fold, and the observed trend replicates finding for the **1a** and **1c** pair (Figure 2). Based on the evaluation results of ligand efficiency and maintained modest potency against HDAC1, we chose compound **7b**, named SS-208, for further investigation.

To fully evaluate the advantage of isoxazole-3-hydroxamates relative to the typical phenylhydroxamate-based HDAC6 inhibitors, we assessed SS-208, **20c**, and NextA against Class I HDACs 1 and 8, Class IIa HDACs 4, 5, 7, and 9, Class IIb HDAC6, and Class IV HDAC11 in-house. The HDAC profiling against Class IIa and Class IV isoforms shows that SS-208 only exhibited micromolar potency against all these isoforms. In the side-by-side comparison with the selective HDAC6i, NextA, SS-208 exhibited similarly low nanomolar HDAC6 inhibitory activity with better selectivity over all the other tested HDAC isoforms (Table 2).

Table 1. HDAC1 and HDAC6 enzymatic evaluation of analogs **7a-d**, **11a-d**, and **20a-c**[a]

Cmpd	cap	CU	ZBG	IC_{50} (μM)		SI[b]	LE[c]	LipE[d]
				HDAC1	HDAC6			
1a[e]	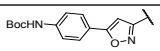		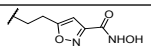	16.9	0.006	2817	0.35	6.2
7a			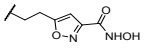	> 30	0.19	> 155	0.47	5.8
7b			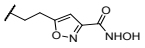	31.5	0.075	418	0.45	5.1
7c			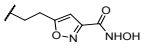	3.03	0.010	294	0.47	5.7
7d	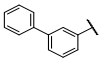		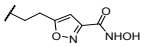	2.04	0.024	85	0.41	5.7
11a			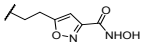	> 30	4.36	> 7	0.31	2.0
11b			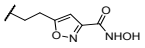	11.2	0.69	16	0.36	3.3
11c			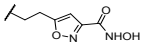	> 30	1.99	> 15	0.31	2.1
11d	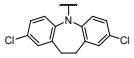		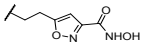	> 30	1.35	> 22	0.27	1.3
20a			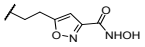	> 30	0.20	> 152	0.45	3.9
20b			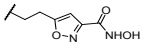	> 30	1.98	> 15	0.38	2.5
20c			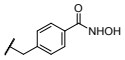	0.20	0.028	7.2	0.48	4.8
NextA[f]			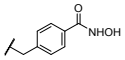	2.86	0.005	572	0.46	5.7
TSA[g]	-	-	-	0.009	0.002	4.4	0.55	6.4

[a]IC_{50} values are the mean of two experiments obtained from curve-fitting of a 10-point enzymatic assay starting from 30 μM with 3-fold serial dilution against HDAC1 and HDAC6 (Reaction Biology Corp, Malvern, PA). [b]SI: HDAC6 selectivity over HDAC1. [c]LE: ligand efficiency = 1.4*pIC_{50}/number of heavy atoms. [d]LipE: lipophilic ligand

efficiency = $pIC_{50} - clog\ P_{o/w}$. [e]IC_{50} values were extracted from the article by Gaisina, I. N. et al., *ChemMedChem* **2016**, *11*, 81-92. [f]IC_{50} values were extracted from the article by Kozikowski, A. P. et al., *ACS Chem. Neurosci.* **2019**, *10*, 1679-1695. [g]TSA: trichostatin A.

Table 2. HDAC profiles of the 3,4-dichlorophenyl capped compounds SS-208 and **20c**, as well as NextA[a]

Cmpd	**SS-208 (7b)**		**20c**		**NextA**	
Structure	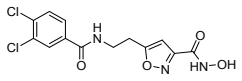		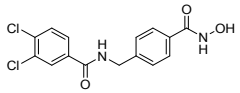		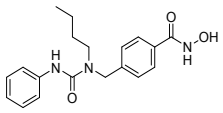	
Isoform	**IC_{50} (μM)**	**SI[b]**	**IC_{50} (μM)**	**SI**	**IC_{50} (μM)**	**SI**
HDAC1	1.39 ± 0.73	116	0.034 ± 0.003	17	0.36 ± 0.12	90
HDAC4	19.5 ± 4.2	1625	3.53 ± 0.13	1765	14.8 ± 1.7	3700
HDAC5	6.91 ± 0.29	576	3.12 ± 0.48	1560	6.62 ± 2.66	1655
HDAC6	0.012 ± 0.002	1	0.002 ± 0.0003	1	0.004 ± 0.002	1
HDAC7	8.34 ± 0.71	695	0.50 ± 0.008	250	2.43 ± 0.30	608
HDAC8	1.23 ± 0.59	103	0.92 ± 0.15	460	1.54 ± 0.76	385
HDAC9	38.2 ± 5.1	3183	3.07 ± 0.17	1535	2.0 ± 0.77	500
HDAC11	5.12 ± 1.29	427	1.05 ± 0.11	525	10.6 ± 2.2	2650

[a]IC_{50} values are the mean of two experiments ± SEM obtained from curve-fitting of a 10-point enzymatic assay starting from 100 μM with 3-fold serial dilution against HDAC isoform. [b]SI: HDAC6 selectivity index over other HDAC isoforms.

Crystallization Studies. The recently published co-crystal structures of phenylhydroxamate-based HDAC6is in complex with drHDAC6 displayed an unusual monodentate phenylhydroxamate-Zn^{2+} coordination geometry, while a bidentate coordination is generally observed for inhibitors that possess either flexible aliphatic linkers or aromatic linkers lacking a cap.[85, 86] The recent findings demonstrated that the caps attached to the phenylhydroxamate affect the coordination between the hydroxamates and the catalytic Zn^{2+} to be bidentate or monodentate, which is also crucial to stabilize the

monodentate coordination mode that is slightly less stable (0.5 kcal/mol) than the bidentate coordination mode.[85, 87] Moreover, the key residues H463, P464, F583, and L712 create an L1-loop pocket to provide a rigid binding site for hydrophobic caps. Recent research further supports that the interaction between ligand and L1-loop pocket is critical for maintaining high selectivity against class I HDACs.[87]

To investigate the molecular basis of interactions between SS-208 and HDAC6, we solved the crystal structure of the drHDAC6-CD2/SS-208 complex to the ultra-high resolution limit of 1.15 Å. Binding of SS-208 to HDAC6 did not cause any major structural rearrangement of the enzyme as documented by the RMSD of 0.15 Å for 300 Cα atoms between the drHDAC6/SS-208 complex and the unliganded enzyme (PDB code: 5EEM).[88] The hydroxamate functional group of SS-208 coordinates the active-site zinc ion in a canonical bidentate fashion, forming a typical five-membered chelate complex with interatomic distances of 2.1 Å between the Zn^{2+} and each of the hydroxamate C=O and N-O groups (Figure 3A). Moreover, the hydroxamate C=O group accepts a hydrogen bond from the hydroxyl group of Y745 (2.7 Å), and the N-O- group forms hydrogen bonds with the side chains of H573 (2.6 Å) and H574 (2.5 Å and 2.9 Å). The isoxazole ring and the distal ethylene part of the linker are positioned within van der Waals distances from the side chains of F583, F643, and L712. The C=O group of the amide moiety establishes an interaction with S531 in a distance of 3.3 Å, and the N-H group engages in a water-mediated interaction with H614 as observed in the binding with other HDAC6is in the literature.[87] Finally, the capping dichlorophenyl ring packs against the hydrophobic patch at the entrance of the internal tunnel, the L1-loop pocket, formed by side chains of H463, P464, F583, and L712 (Figure 3B).[87]

It is interesting to note that the bidentate zinc ion coordination reported here differs from the preferred monodentate coordination observed in drHDAC6 complexes where a phenylhydroxamate group is capped by a hydrophobic moiety of an inhibitor.[40, 85, 87] In our complex, the center of the isoxazole ring is shifted by 0.5 Å towards the active-site Zn^{2+}, and this shift stems from the bidentate coordination of the Zn^{2+} by the hydroxamate moiety (Figure 3C). This shift is likely facilitated by the presence of a "long" four-atom linker between the isoxazole ring and the capping dichlorophenyl moiety, allowing thus for the more energetically favorable bidentate hydroxamate coordination while simultaneously preserving hydrophobic interactions between the cap and the L1-loop pocket.[87]

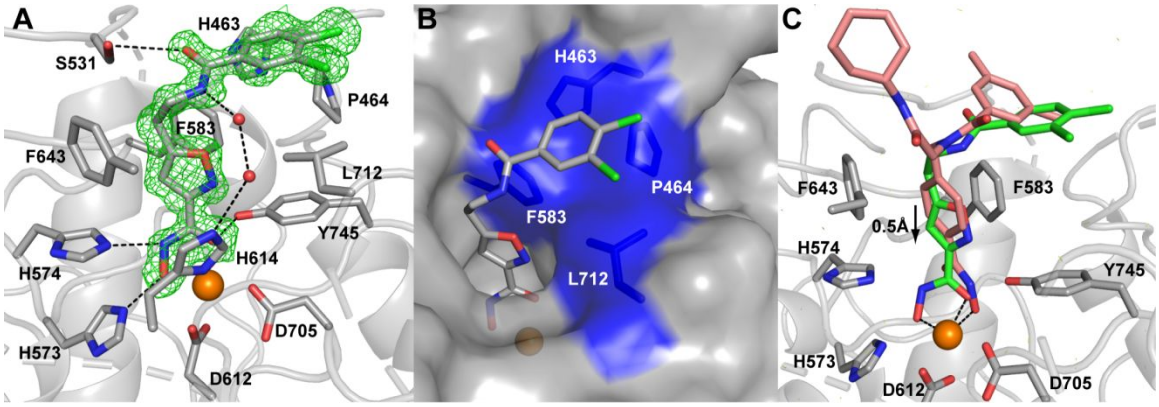

Figure 3. Crystal structure of the drHDAC6−CD2/SS-208 complex. (A) Detail view of the substrate tunnel of HDAC6 in complex with SS-208. *Fo-Fc* maps (green mesh) for SS-208 are contoured at 4.0 σ and the inhibitor and selected HDAC6 residues are shown in stick representation with atoms colored grey (carbon), red (oxygen), blue (nitrogen), and green (chlorine). The active-site zinc ion and water molecules are shown as orange and red spheres, respectively. H-bonds and salt bridges are shown as dashed lines. (B) Interactions between the capping dichlorophenyl moiety and the "L1-loop pocket" formed by side chains of H463, P464, F583, and L712 (colored blue). The surface of HDAC6 is shown in

semi-transparent surface representation. (C) Superposition of SS-208 and DDK-115 (PDB code: 6DVL) in the substrate tunnel of HDAC6. Carbon atoms are colored green and pink for SS-208 and DDK-115, respectively. The active-site zinc ion is coordinated in a bidentate fashion by SS-208, while monodentate coordination is observed for DDK-115, resulting in the 0.5 Å shift of the SS-208 ring closer towards the zinc ion.

HDAC target engagement measurement in HEK293 cells. We further assessed the potency and selectivity of SS-208 in live cells using NanoBERT target engagement assay to investigate its binding characteristics with HDAC1 and HDAC6 within intact cells.[89] These results performed in HEK293 are summarized in Figure 4, and suggest that SS-208 retains modest activity against HDAC1 in cells (IC_{50} = 6.67 μM), while the measured potency of SS-208 against the α-tubulin preferring deacetylase domain of HDAC6, the catalytic domain 2 (IC_{50} = 0.5 μM), indicates SS-208 retains about 13-fold selectivity over HDAC1 in cells (418-fold enzymatic selectivity over HDAC1 in Table 1) which is comparable with our recent observation on another highly selective HDAC6i, SW-100, tested under the same conditions.[63] SW-100 showed an IC_{50} value of 2.3 nM against HDAC6 and 2273-fold selectivity over HDAC1 in the enzymatic assay, while it exhibited IC_{50} of 0.10 μM against HDAC6-CD2 and 46-fold selectivity over HDAC1 in the cellular target engagement assay.[63] Vorinostat (SAHA), tested as positive control, demonstrated to be potent and non-selective towards HDAC6-CD2 (IC_{50} = 0.24 μM) as well as HDAC1 (IC_{50} = 0.12 μM) (Figure 4).

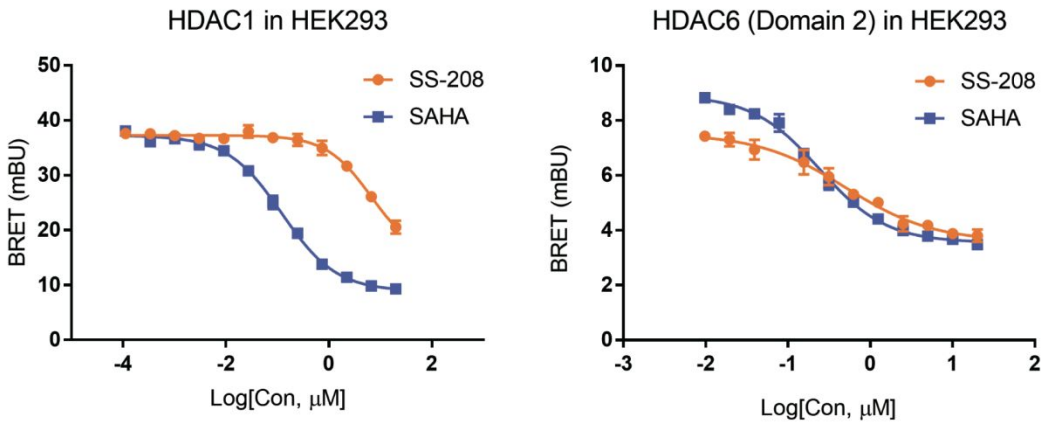

	IC_{50}, μM	
	SS-208	**SAHA**
HDAC1	6.673	0.122
HDAC6-CD2	0.504	0.241

Figure 4. SS-208 selectively inhibits HDAC6-CD2 in cells. HDAC1 and HDAC6 (catalytic domain 2) NanoBRET target engagement assay for compound SS-208 in HEK293. IC_{50} values are the mean of four technical replicates ± SD obtained from curve-fitting of a 12-point engagement assay starting from a concentration of 20 μM with 3-fold serial dilution. SAHA was used as a positive control.

Initial ADMET properties. To evaluate the potential mutagenicity of this hydroxamate-based compound, SS-208 was incubated with two strains of *Salmonella typhimurium* (TA98 and TA1537) in the presence and absence of mammalian microsomal enzymes (S9 mix). SS-208 did not induce ≥ 2-fold increases (for tester strain TA98) or ≥ 3-fold increases (for tester strain TA1537) in the mean number of revertant colonies at any dose levels when compared to the concurrent negative/solvent control, both in the presence and absence of the S9 mix, thus supporting the lack of mutagenicity of SS-208 under the conditions of the Ames assay (Table S3). No significant inhibition was observed in the hERG assay up to

30 μM (Figure S1). The liver microsomal stability is shown in Table 3 (half-lives of 37 min and 135 min in mouse and human microsomes, respectively). This constitutes an improvement relative to the original compound **1a**. Moreover, half-lives of 22 min and 135 min in mouse and human hepatocytes were determined, respectively.

Table 3. Initial ADMET profiling of compound SS-208.[a]

Ames test (with and without S9)	TA98, TA1537	Negative
hERG test (IC_{50}, μM)	HEK293 cells	> 30
Liver microsomal stability ($t_{1/2}$ min, with NADPH)	Mouse	37
	Human	135
Hepatocytes stability ($t_{1/2}$ min)	Mouse	22
	Human	108

[a]All the ADMET assays were conducted by Pharmaron, Inc., Irvine, CA.

Inhibitory potency of SS-208 is comparable to NextA and TubA in cancer cells. As mentioned before, several selective HDAC6is are currently available for pre-clinical research. Among them, NextA and tubastatin A (TubA) were reported by our group.[55, 56] Although these two compounds have shown outstanding *in vivo* anti-tumor effects in numerous syngeneic tumor models,[24] they were found to be Ames-positive (data are not shown). We thus wanted to compare the Ames-negative HDAC6i SS-208 with these two previously reported HDAC6is. We performed an initial screening of the *in vitro* activity of SS-208 by evaluating the acetylation status of α-tubulin (Ac-α-Tubulin), the best characterized physiological substrate of HDAC6. As expected, SS-208 increased Ac-α-Tubulin levels in SM1 murine melanoma (Figure 5A) and WM164 human melanoma (Figure 5B). Additionally, SS-208 had a negligible effect on the levels of acetylated histone H3 (Ac-H3) in SM1 murine melanoma cells, and these findings are comparable to results

of experiments where NextA was used (Figure 5C).

We previously observed that the selective HDAC6is NextA and TubA had similar *in vitro* HDAC inhibitory potency across different human and murine cancer cell lines.[28] A similar outcome was observed with SS-208, which was also comparable to the above mentioned selective HDAC6is when tested in human PC3, human 5637, human T24, and mouse SM1 cell lines (Figure 5D). We also observed that SS-208 induced minimal cell death in the concentration range evaluated above, and these results were also comparable to NextA and TubA (Figure 5E). Importantly, we have reported that the *in vivo* antitumor effect of selective HDAC6is is mainly mediated by their role as modulators of anti-tumor immune responses and that their direct cytotoxicity towards cancer cells is minimal at concentrations lower than 5 μM.[28] Supporting these previously reported findings, we observed that SS-208 has marginal effects on viability, cytotoxicity, and apoptosis in murine SM1 melanoma cells evaluated by the multiplexed Apotox™ assay (Figure 5F). The absence of cytotoxic effects in cells treated with these selective HDAC6is is in sharp contrast to the effects observed with other pan-HDACis such as panobinostat (LBH589 in Figure 5F), among others, therefore removing one of the most critical side effects of non-selective HDACis or other cytotoxic anticancer drugs.

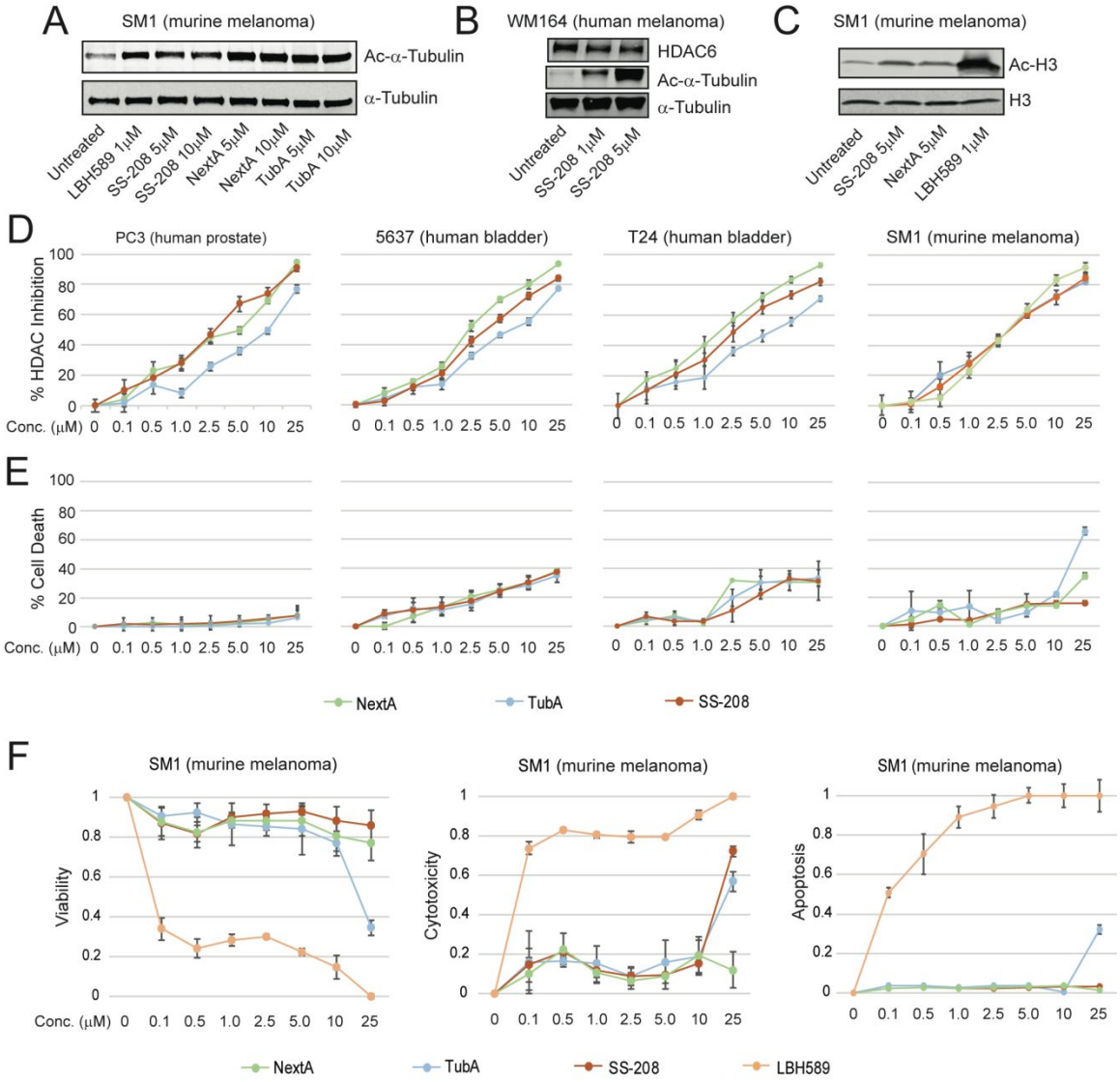

Figure 5. SS-208 activity is similar to other selective HDAC6is in cancer cells *in vitro*. (A) SS-208 treatment of SM1 murine melanoma cells resulted in increased Ac-α-Tubulin similar to other HDAC6is NextA and TubA. (B) The activity of HDAC6 inhibition with SS-208 was dose-dependent as indicated by Western-blot analysis of Ac-α-Tubulin in WM164 human melanoma cells. (C) SM1 melanoma cells were treated with SS-208, NextA, or LBH589 for 24 h. The levels of Ac-H3 were evaluated by Western-blot analysis. (D) SS-208, NextA, and TubA exhibited similar inhibition of deacetylase activity when tested in a panel of cell lines of various tissue origins. (E) Similarly, HDAC6is did not

induce cell death across the range of concentrations tested. (F) Multiplexed assay indicated that pan-HDACi, LBH589 exhibited apoptosis and cytotoxicity at concentrations as low as 100 nM, while the HDAC6is tested did not affect cell viability up to 10 μM. HDAC6is also did not induce apoptosis and cytotoxicity compared to LBH589.

SS-208 reduces the expression of PD-L1 in melanoma cells. Our group has previously reported that the genetic and pharmacological targeting of HDAC6 affected the expression of the immunosuppressive molecule PD-L1 (CD274). Abrogation of HDAC6 activity results in inactivation of the STAT3 pathways upon treatment with HDAC6is or knockdown of HDAC6.[50] To further evaluate if SS-208 affects the processes mentioned above, we evaluated the activation of the STAT3 pathway by assessing the phosphorylation of STAT3 after treatment with SS-208 (5 μM). Western blot results illustrated in Figure 6A demonstrated that SS-208 efficiently reduced IL-6-mediated Y705 phosphorylation of STAT3 and the subsequent downregulation of the PD-L1 expression. HDAC6 inhibition was evidenced by the increased levels of Ac-α-Tubulin. Further verification by qRT-PCR indicated that IL-6 significantly increased CD274 gene expression by at least 2-fold compared to the untreated condition, and SS-208 effectively negated IL-6 induced CD274 gene expression suggesting that this HDAC6i regulates PD-L1 expression at the mRNA level rather than through post-translational modifications at the protein level (Figure 6B).

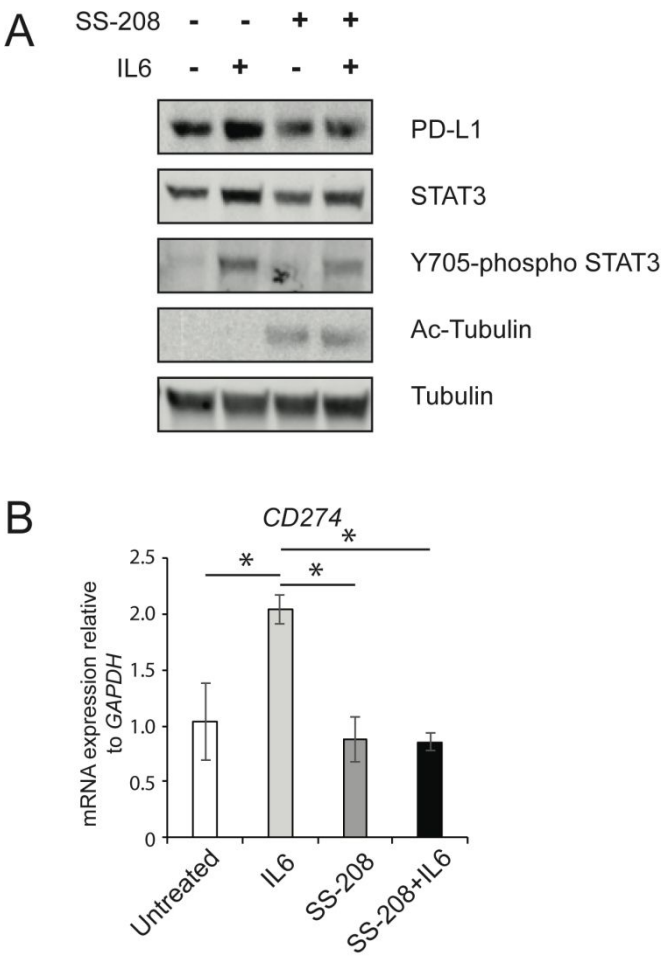

Figure 6. Immunomodulatory role of SS-208 by decreasing the expression of PD-L1 in melanoma cells. (A) SM1 murine melanoma cells pre-treated with 5 μM of SS-208 followed by IL-6 treatment for overnight effectively reduced the expression of immunosuppressive molecule PD-L1 at the protein level. (B) SS-208 decreased IL-6 mediated STAT3 activation measured as Y705 phosphorylation and subsequently PD-L1 gene expression measured by qRT-PCR.

SS-208 impairs melanoma tumor growth in immunocompetent mice. The *in vivo* antitumor effect of selective HDAC6is has been extensively investigated.[35, 50, 51] Importantly, this activity needs the presence of an intact host immune system.[28] Therefore, we wanted to evaluate whether SS-208 could also impair tumor growth in a syngeneic

murine model with a functional immune system. To evaluate this possibility, we injected immunogenic murine SM1 melanoma cells subcutaneously in the flank of C57BL/6 mice and subsequently treated them with SS-208 (25 mg/kg, ip administration) or vehicle after one-week post tumor engraftment. As observed previously for other HDAC6is, the tumor growth was significantly reduced after treatment with SS-208 (Figure 7A-B), suggesting that this Ames-negative selective HDAC6i also exerts its anti-tumor effect by modulating the host immune system. To test this hypothesis, we evaluated the composition of different cellular components of the TME. Although we did not observe a significant infiltration of cytotoxic T cells (CD8+), their presence in the TME was slightly superior to the vehicle control (Figure 7C). Among other screened tumor-infiltrating lymphocytes (TILs), the infiltration of CD4+ T cells did not change (Figure 7D). However, the infiltration of natural killer T cells (NKT) was significantly upregulated in the SS-208 treatment arm (Figure 7E).

The anti-tumoral M1 macrophage phenotype has been reported to be associated with better prognosis in several malignancies, and there is an active search for agents improving their infiltration in tumors[90] On the other hand, tumor infiltration of pro-tumoral M2 macrophages is directly associated with a bad prognosis in cancer.[91] In previous studies from our group, we observed a significant increase in the ratio of M1 and M2 macrophages in tumors treated with selective HDAC6is but not with other non-selective inhibitors.[51] As expected, this outcome was also observed in the melanomas of the mice treated with SS-208 (Figure 7F-H), confirming that this compound possesses similar immunological properties as previously investigated NextA.[48]

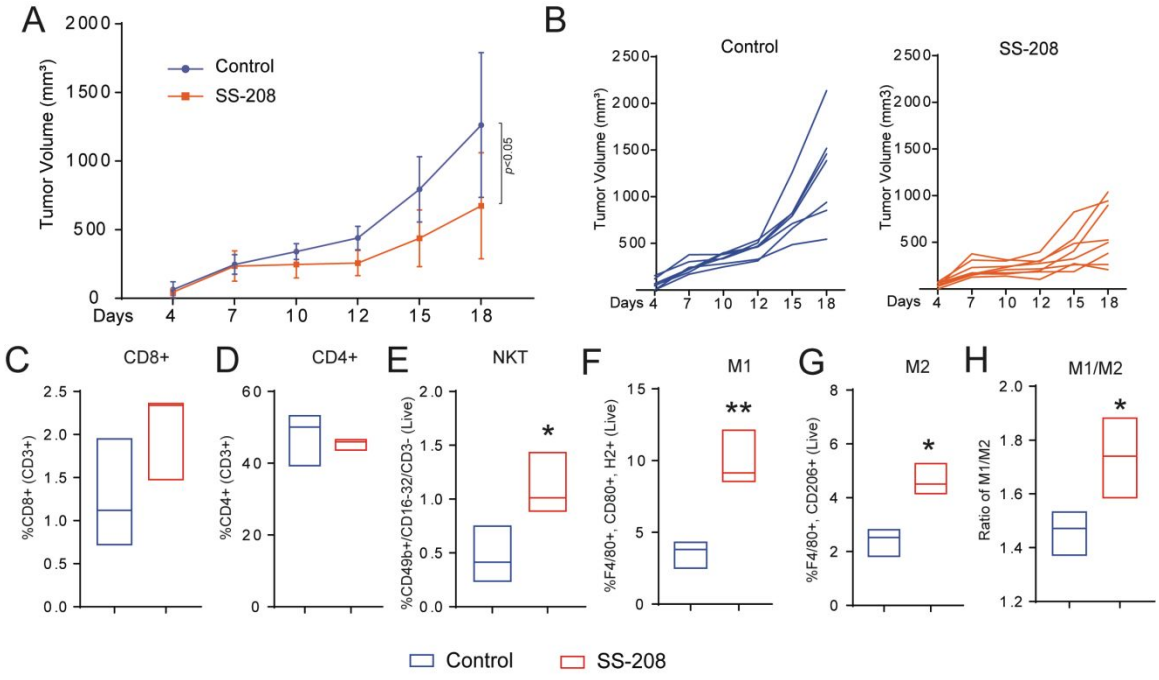

Figure 7. *In vivo* anti-tumor activity of SS-208 is mediated through modulation of tumor microenvironment. (A) SS-208 treatment (25 mg/kg, ip) significantly decreased the tumor growth compared to the control group in SM1 murine melanoma syngeneic model. (B) Tumor growth curves of individual animals in control and SS-208 treatment groups. Animals receiving SS-208 treatment consistently showed lower tumor volume during the course of study compared to control groups. The decrease in tumor volume in the SS-208 treatment group was associated with infiltration of intra-tumoral CD8+ T-cells (C), CD4+ T-cells (D), and significant increase in NKT-cells (E). SS-208 treatment was associated with significant increase in anti-tumor M1 macrophages (F), M2 macrophages (G), and the ratio of M1/M2 (H) which is an indication of effective anti-tumor immunity.

CONCLUSIONS.

We have designed and synthesized a series of HDAC6 inhibitors bearing isoxazole-3-

hydroxamate instead of phenylhydroxamate as ZBG. By evaluating their inhibitory activities at HDAC isoforms, we found that: (a) the amide moiety is an important constituent of the connecting unit to retain high HDAC6 potency; (b) bulky caps, like napththyl and biphenyl groups, result in better HDAC6 activity but lower selectivity *versus* HDAC1; (c) the replacement of the corresponding phenylhydroxamate leads to the significant potency improvement against HDAC6 but the loss of hundred-fold HDAC1 selectivity. We have thus identified a novel potent and selective HDAC6i, namely SS-208. The X-ray structure analysis of the crystallized complex of SS-208 with catalytic domain 2 from *Danio rerio* HDAC6 demonstrates that: (a) the hydroxamate moiety coordinates in a distinct bidentate manner with the active-site zinc ion, forming a typical five-membered chelate complex, in contrast to the preferred monodentate coordination observed in most HDAC6 complexes with phenylhydroxamate-based inhibitors; (b) direct and indirect engagements are observed between the key amide moiety and amino acid residues in the active site that may be responsible for the ligand's nanomolar HDAC6 potency; (c) the interactions between the 3,4-dichlorophenyl cap and the L1-loop pocket is critical for high selectivity against HDAC1. Both *in vitro* and *in vivo* ADMET profiling and pharmacological observation suggest that: (a) SS-208 shows Ames-negative results under the testing conditions and no significant inhibition in the hERG assay, and is more metabolically stable relative to the original compound **1a**; (b) In murine and human melanoma cells, SS-208 induces minimal cell death and exhibits marginal effects on viability, cytotoxicity, and apoptosis, while significantly increases the levels of Ac-α-Tubulin; (c) Furthermore, SS-208 efficiently reduces the IL-6-mediated Y705 phosphorylation of STAT3 and downregulates the expression of PD-L1 at the mRNA

levels in melanoma cells; (d) Finally, SS-208 impairs tumor growth in a murine SM1 syngeneic melanoma mouse model which is mainly mediated by immune-related antitumor activity as evidenced by the increased infiltration of CD8+ and NK+ T cells and the enhanced ratio of M1 and M2 macrophages in the TME.

Experimental section.

Chemistry

General information. ^{1}H and ^{13}C NMR spectra were obtained on 400/101 and 500/126 MHz Bruker spectrometers, except where noted otherwise, using the solvent residual peak as the internal reference (chemical shifts: $CDCl_3$, δ 7.26/77.0; DMSO-d_6, 2.50/39.52; acetone-d_6, 2.05/29.84 and 206.26). The following abbreviations for multiplicities were used: s = singlet, d = doublet, t = triplet, q = quartet, p = pentet, m = multiplet, dd = double doublet, dt = double triplet, ddd = double-double doublet, and br s = broad singlet. TLC plates (Merck silica gel 60 F_{254}, 250 μm thickness) were used to monitor reaction progress, and spots were visualized under UV (254 nm). High-resolution mass spectrometry (HRMS) was carried out on a Shimadzu IT-TOF instrument under the following conditions: column, ACE 3AQ (50 × 2.1 mm, id); mobile phase, 5 – 100% acetonitrile/water containing 0.1% formic acid at a flow rate of 0.5 mL/min for 4 min. Flash chromatography was performed on a Combi-Flash Rf system (Teledyne ISCO) with silica gel cartridges. Preparative HPLC was used in the purification of all final compounds using a Shimadzu preparative LC under the following conditions: column, ACE 5AQ (150 × 21.2 mm, id); mobile phase: 5 – 100% acetonitrile/water containing 0.05% TFA at a flow rate of 17 mL/min for 30 min; UV detection at 254 and 280 nm. Analytical HPLC was used to determine the purity of all final products using an Agilent 1260 series instrument under the

following conditions: column, ACE 3 (150 × 4.6 mm, id); mobile phase, 5 – 100% acetonitrile/water containing 0.05% TFA at a flow rate of 1.0 mL/min for 25 min; UV detection at 254 nm. The purity of all tested compounds for *in vitro* biological studies was >95%. The purity of SS-208 for crystallographic and *in vivo* studies was >98%.

2-(But-3-yn-1-yl)isoindoline-1,3-dione (3). To a stirred solution of 3-butyn-1-ol (**2a**, 140 mg, 2.0 mmol), phthalimide (382 mg, 2.6 mmol), and Ph_3P (682 mg, 2.6 mmol) was added DEAD (525 mg, 2.6 mmol) at 0 °C under an argon atmosphere. The resulting mixture was slowly warmed to room temperature and stirred at the same temperature for 2.5 h. Then the reaction was quenched with H_2O and extracted with EtOAc (20 mL × 3). The combined organic extracts were washed with brine (40 mL), dried over Na_2SO_4, and concentrated under vacuum. The crude product was purified by flash chromatography (0 – 50% EtOAc/hexane) to afford **3** as a white powder (370 mg, 93%). ^{1}H NMR (400 MHz, $CDCl_3$) δ 7.86 (dd, *J* = 5.5, 3.0 Hz, 2H), 7.73 (dd, *J* = 5.5, 3.0 Hz, 2H), 3.89 (t, *J* = 7.1 Hz, 2H), 2.62 (td, *J* = 7.1, 2.7 Hz, 2H), 1.96 (t, *J* = 2.7 Hz, 1H). ^{13}C NMR (101 MHz, $CDCl_3$) δ 168.0, 134.1, 132.0, 123.4, 80.3, 70.3, 36.6, 18.4.

N*-(But-3-yn-1-yl)benzamide (5a)**. ***General Procedure A: (i) To a stirred solution of **3** (180 mg, 0.9 mmol) in MeOH (5 mL) was added hydrazine monohydrate (0.06 mL, 1.13 mmol). The resulting mixture was stirred at room temperature for 16 h. The precipitate was filtered off, and the filtrate was diluted with water (5 mL) and acidified to pH = 2 with 2 N HCl. The solution was concentrated under vacuum to afford **4** as a white powder. The crude product was used directly in the next step. (ii) To a stirred solution of **4** in DCM (5 mL) were added TEA (0.37 mL, 2.7 mmol) and benzoyl chloride (252 mg, 1.8 mmol) at 0 °C. Then the resulting mixture was stirred at the same temperature for 30 min. The reaction

was quenched with water (5 mL), and the mixture was extracted with DCM (10 mL × 3). The combined organic extracts were washed with brine (40 mL), dried over Na_2SO_4, and concentrated under vacuum. The crude product was purified by flash chromatography (0 – 50% EtOAc/hexane) to afford **5a** as a white powder (140 mg, 90%). ^{1}H NMR (400 MHz, acetone-d_6) δ 7.94 – 7.92 (m, 3H), 7.58 – 7.53 (m, 1H), 7.52 – 7.45 (m, 2H), 3.57 (td, J = 7.1, 6.0 Hz, 2H), 2.55 (td, J = 7.1, 2.7 Hz, 2H), 2.43 (t, J = 2.7 Hz, 1H).

N*-(But-3-yn-1-yl)-3,4-dichlorobenzamide (5b)** was synthesized from **3** (260 mg, 1.3 mmol) and 3,4-dichlorobenzoyl chloride (543 mg, 2.6 mmol) following ***General Procedure A and was obtained as a colorless solid (220 mg, 70%). ^{1}H NMR (400 MHz, $CDCl_3$) δ 7.88 (d, J = 2.0 Hz, 1H), 7.60 (dd, J = 8.3, 2.1 Hz, 1H), 7.52 (d, J = 8.3 Hz, 1H), 6.41 (s, 1H), 3.61 (q, J = 6.2 Hz, 2H), 2.53 (td, J = 6.3, 2.6 Hz, 2H), 2.07 (t, J = 2.6 Hz, 1H).

Ethyl 5-(2-Benzamidoethyl)isoxazole-3-carboxylate (6a). ***General Procedure B***: To a solution of **5a** (140 mg, 0.8 mmol) in EtOAc (2 mL) were added $NaHCO_3$ (201 mg, 2.4 mmol) and ethyl 2-chloro-2-(hydroxyimino)acetate (367 mg, 2.4 mmol) in a microwave reaction tube. The mixture was heated at 100 °C for 1 h in a microwave reactor. After completion of the reaction, the solid was filtered off and the filtrate was concentrated under reduced pressure. The crude product was purified by flash chromatography (0 – 50% EtOAc/hexane) to afford **6a** as a colorless oil (140 mg, 61%). ^{1}H NMR (400 MHz, $CDCl_3$) δ 7.74 (dt, J = 7.1, 1.3 Hz, 2H), 7.55 – 7.46 (m, 1H), 7.46 – 7.36 (m, 2H), 6.51 (s, 2H), 4.42 (q, J = 7.1 Hz, 2H), 3.82 (q, J = 6.4 Hz, 2H), 3.19 (t, J = 6.5 Hz, 2H), 1.40 (t, J = 7.1 Hz, 3H). ^{13}C NMR (101 MHz, $CDCl_3$) δ 172.7, 167.8, 159.9, 156.6, 134.1, 131.8, 128.7, 126.9, 102.7, 62.2, 37.9, 27.2, 14.1.

Ethyl 5-(2-(3,4-Dichlorobenzamido)ethyl)isoxazole-3-carboxylate (6b) was synthesized from **5b** (220 mg, 0.9 mmol) and ethyl 2-chloro-2-(hydroxyimino)acetate (408 mg, 2.7 mmol) following ***General Procedure B*** and was obtained as a white solid (250 mg, 78%). ^{1}H NMR (400 MHz, DMSO-d_6) δ 8.85 (t, J = 5.5 Hz, 1H), 8.03 (d, J = 1.4 Hz, 1H), 7.82 – 7.71 (m, 2H), 6.76 (s, 1H), 4.34 (q, J = 7.1 Hz, 2H), 3.60 (q, J = 6.5 Hz, 2H), 3.11 (t, J = 6.7 Hz, 2H), 1.30 (t, J = 7.1 Hz, 3H). ^{13}C NMR (101 MHz, DMSO-d_6) δ 173.5, 164.2, 159.6, 156.1, 134.6, 134.2, 131.3, 130.8, 129.2, 127.5, 102.5, 61.8, 37.4, 26.3, 14.0.

Ethyl 5-(2-(2-Naphthamido)ethyl)isoxazole-3-carboxylate (6c). (i) **5c** was synthesized from **3** (215 mg, 1.08 mmol) and 2-naphthoyl chloride (246 mg, 1.3 mmol) following ***General Procedure A*** and was obtained as a white powder (170 mg, 70%); (ii) **6c** was synthesized from **5c** (170 mg, 0.76 mmol) and ethyl 2-chloro-2-(hydroxyimino)acetate (344 mg, 2.28 mmol) following ***General Procedure B*** and was obtained as a white solid (150 mg, 58%).^{1}H NMR (400 MHz, $CDCl_3$) δ 8.25 (s, 1H), 7.86 – 7.77 (m, 4H), 7.57 – 7.45 (m, 2H), 6.90 (t, J = 5.7 Hz, 1H), 6.50 (s, 1H), 4.38 (q, J = 7.1 Hz, 2H), 3.85 (q, J = 6.5 Hz, 2H), 3.20 (t, J = 6.6 Hz, 2H), 1.36 (t, J = 7.1 Hz, 3H).

Ethyl 5-(2-(Biphenyl-3-ylcarboxamido)ethyl)isoxazole-3-carboxylate (6d). (i) **5d** was synthesized from **3** (215 mg, 1.08 mmol) and biphenyl-3-carbonyl chloride (280 mg, 1.3 mmol) following ***General Procedure A*** and was obtained as a white powder (140 mg, 52%). (ii) **6d** was synthesized from **5d** (170 mg, 0.56 mmol) and ethyl 2-chloro-2-(hydroxyimino)acetate (255 mg, 1.69 mmol) following ***General Procedure B*** and was obtained as a colorless oil (100 mg, 49%). ^{1}H NMR (400 MHz, $CDCl_3$) δ 7.98 (s, 1H), 7.76 – 7.65 (m, 2H), 7.58 – 7.51 (m, 2H), 7.45 – 7.38 (m, 3H), 7.36 – 7.30 (m, 1H), 7.06 (t, J = 5.4 Hz, 1H), 6.47 (s, 1H), 4.35 (q, J = 7.1 Hz, 2H), 3.78 (q, J = 6.5 Hz, 2H), 3.14 (t, J = 6.6

Hz, 2H), 1.33 (t, J = 7.1 Hz, 3H).

5-(2-Benzamidoethyl)-*N*-hydroxyisoxazole-3-carboxamide (7a). ***General Procedure C***: In a round bottom flask, NaOH (160 mg, 4.0 mmol) was dissolved in 50% aqueous NH_2OH (1.6 mL, approx. 50 equiv.) at 0 °C. A solution of **6a** (140 mg, 0.5 mmol) in 1:1 THF/MeOH (6 mL) was added dropwise and stirring was continued for 30 min while the mixture was allowed to warm to room temperature. The solution was neutralized with 2N HCl and extracted with EtOAc (15 mL × 3). The comnbined organic layers were washed with brine, dried over Na_2SO_4, and concentrated under vacuum. The crude product was purified by flash chromatography (0 – 10% MeOH/DCM) or preparative HPLC and lyophilized to afford **7a** as a white powder (60 mg, 43%). ^{1}H NMR (400 MHz, DMSO-d_6) δ 8.68 (t, J = 5.5 Hz, 1H), 7.81 (d, J = 7.1 Hz, 2H), 7.53 (t, J = 7.3 Hz, 1H), 7.46 (t, J = 7.3 Hz, 2H), 6.63 (s, 1H), 3.60 (q, J = 6.6 Hz, 2H), 3.09 (t, J = 6.7 Hz, 2H). ^{13}C NMR (101 MHz, DMSO-d_6) δ 172.4, 166.4, 157.4, 156.2, 134.3, 131.3, 128.3 (2C), 127.1 (2C), 101.1, 37.2, 26.3. ESI HRMS calc. for $C_{13}H_{14}N_3O_4$: $[M+H]^+$, m/z 276.0979; found: 276.0984.

5-(2-(3,4-Dichlorobenzamido)ethyl)-*N*-hydroxyisoxazole-3-carboxamide (7b, SS-208) was synthesized from **6b** (250 mg, 0.7 mmol) following ***General Procedure C*** and was obtained as a white powder (70 mg, 29%). ^{1}H NMR (400 MHz, DMSO-d_6) δ 11.46 (s, 1H), 9.33 (s, 1H), 8.87 (t, J = 5.3 Hz, 1H), 8.04 (d, J = 1.6 Hz, 1H), 7.83 – 7.72 (m, 2H), 6.63 (s, 1H), 3.59 (q, J = 6.4 Hz, 2H), 3.09 (t, J = 6.8 Hz, 2H). ^{13}C NMR (101 MHz, DMSO-d_6) δ 172.3, 164.1, 157.4, 156.2, 134.5, 134.1, 131.3, 130.8, 129.1, 127.5, 101.2, 37.4, 26.1. ESI HRMS calc. for $C_{13}H_{12}Cl_2N_3O_4$: $[M+H]^+$, m/z 344.0205; found: 344.0198. Purity: 98.8% (254 nm).

5-(2-(2-Naphthamido)ethyl)-*N*-hydroxyisoxazole-3-carboxamide (7c) was synthesized

from **6c** (150 mg, 0.44 mmol) following ***General Procedure C*** and was obtained as a white powder (15 mg, 10%). ^{1}H NMR (400 MHz, DMSO-d_6) δ 11.45 (br s, 1H), 9.33 (br s, 1H), 8.85 (t, J = 5.2 Hz, 1H), 8.41 (s, 1H), 8.03 – 7.88 (m, 3H), 7.90 (d, J = 8.6 Hz, 1H), 7.63 – 7.57 (m, 2H), 6.66 (s, 1H), 3.66 (q, J = 6.5 Hz, 2H), 3.14 (t, J = 6.7 Hz, 2H). ESI HRMS calc. for $C_{17}H_{16}N_3O_4$: $[M+H]^+$, m/z 326.1135; found: 326.1137.

5-(2-([1,1'-Biphenyl]-3-ylcarboxamido)ethyl)-*N*-hydroxyisoxazole-3-carboxamide (7d) was synthesized from **6d** (100 mg, 0.27 mmol) following ***General Procedure C*** and was obtained as an off-white powder (30 mg, 32%). ^{1}H NMR (400 MHz, DMSO-d_6) δ 11.47 (br s, 1H), 9.33 (br s, 1H), 8.81 (t, J = 5.6 Hz, 1H), 8.08 (s, 1H), 7.82 (t, J = 7.4 Hz, 2H), 7.72 (d, J = 7.4 Hz, 2H), 7.56 (t, J = 7.7 Hz, 1H), 7.50 (t, J = 7.6 Hz, 2H), 7.41 (t, J = 7.1 Hz, 1H), 6.64 (s, 1H), 3.63 (q, J = 6.5 Hz, 2H), 3.12 (t, J = 6.8 Hz, 3H). ESI HRMS calc. for $C_{19}H_{16}N_3O_4$: $[M–H]^+$, m/z 350.1146; found: 350.1136.

Ethyl 5-(4-Hydroxybutyl)isoxazole-3-carboxylate (8a) was synthesized from 5-hexyn-1-ol (**2b**, 200 mg, 2.0 mmol) and ethyl 2-chloro-2-(hydroxyimino)acetate (906 mg, 6.0 mmol) following ***General Procedure B*** and was obtained as a colorless oil (370 mg, 87%). ^{1}H NMR (400 MHz, $CDCl_3$) δ 6.41 (s, 1H), 4.42 (qd, J = 7.1, 1.3 Hz, 2H), 3.68 (td, J = 6.3, 1.3 Hz, 2H), 2.84 (t, J = 7.5 Hz, 2H), 1.90 – 1.76 (m, 2H), 1.67 – 1.60 (m, 2H), 1.40 (td, J = 7.1, 1.3 Hz, 3H). ^{13}C NMR (101 MHz, $CDCl_3$) δ 175.4, 160.3, 156.5, 101.7, 62.3, 62.2, 31.9, 26.6, 23.9, 14.3.

Ethyl 5-(3-Hydroxypropyl)isoxazole-3-carboxylate (8b) was synthesized from 4-pentyn-1-ol (**2c**, 300 mg, 3.57 mmol) and ethyl 2-chloro-2-(hydroxyimino)acetate (1.6 g, 10.7 mmol) following ***General Procedure B*** and was obtained as a colorless oil (680 mg, 96%). ^{1}H NMR (400 MHz, $CDCl_3$) δ 6.42 (s, 1H), 4.40 (q, J = 7.1 Hz, 2H), 3.70 (t, J = 6.1

Hz, 2H), 2.92 (t, J = 7.6 Hz, 2H), 1.97 – 1.88 (m, 2H), 1.38 (t, J = 7.1 Hz, 3H). ^{13}C NMR (101 MHz, $CDCl_3$) δ 175.2, 160.3, 156.5, 101.8, 62.2, 61.3, 30.2, 23.3, 14.2.

Ethyl 5-(4-Bromobutyl)isoxazole-3-carboxylate (9a). To a stirred solution of **8a** (100 mg, 0.47 mmol) in DCM (5 mL) were added CBr_4 (232 mg, 0.47 mmol) and Ph_3P (184 mg, 0.47 mmol) at 0 °C. Then the resulting mixture was stirred at room temperature for 1 h. The reaction was quenched with water (5 mL) and extracted with DCM (15 mL × 3). The combined organic extracts were washed with brine (30 mL), dried over Na_2CO_3, and concentrated under vacuum. The crude product was purified by flash chromatography (0 – 40% EtOAc/hexane) to afford **9a** as a colorless oil (90 mg, 89%).^{1}H NMR (400 MHz, $CDCl_3$) δ 6.41 (s, 1H), 4.40 (q, J = 7.1 Hz, 2H), 3.40 (t, J = 6.2 Hz, 2H), 2.83 (t, J = 6.9 Hz, 2H), 1.89 – 1.87 (m, 4H), 1.38 (t, J = 7.1 Hz, 3H). ^{13}C NMR (101 MHz, $CDCl_3$) δ 174.7, 160.2, 156.5, 101.8, 62.1, 32.8, 31.8, 26.0, 25.9, 14.2.

Ethyl 5-(4-Oxobutyl)isoxazole-3-carboxylate (9b). To a stirred solution of **8a** (150 mg, 0.70 mmol) in DCM (5 mL) was added pyridinium chlorochromate (300 mg, 1.4 mmol) at room temperature. The resulting mixture was stirred at the same temperature for 2 h. Then the solid was filtered off and the filtrate was concentrated under vacuum. The crude product was purified by flash chromatography (0 – 60% EtOAc/hexane) and **9b** was obtained as a colorless oil (130 mg, 88%). ^{1}H NMR (400 MHz, $CDCl_3$) δ 9.75 (t, J = 1.1 Hz, 1H), 6.40 (s, 1H), 4.38 (q, J = 7.1 Hz, 2H), 2.83 (t, J = 7.3 Hz, 2H), 2.53 (td, J = 7.1, 1.0 Hz, 2H), 2.11 – 1.94 (m, 2H), 1.36 (t, J = 7.1 Hz, 3H). ^{13}C NMR (101 MHz, $CDCl_3$) δ 200.9, 174.3, 160.1, 156.5, 101.9, 62.1, 42.6, 25.8, 19.8, 14.1.

Ethyl 5-(3-Bromopropyl)isoxazole-3-carboxylate (9c) was synthesized from **8b** (680 mg, 3.42 mmol), CBr_4 (1.70 g, 5.13 mmol), and Ph_3P (1.35 g, 5.13mmol) using a procedure

similar to that described for the synthesis of **9a** and was obtained as a colorless oil (850 mg, 83%). ^{1}H NMR (400 MHz, $CDCl_3$) δ 6.46 (s, 1H), 4.42 (q, *J* = 7.1 Hz, 2H), 3.43 (t, *J* = 6.3 Hz, 2H), 3.01 (t, *J* = 7.3 Hz, 2H), 2.33 – 2.18 (m, 2H), 1.40 (t, *J* = 7.1 Hz, 3H). ^{13}C NMR (101 MHz, $CDCl_3$) δ 173.6, 160.1, 156.6, 102.3, 62.3, 31.9, 30.2, 25.3, 14.3.

Ethyl 5-(4-(5,6-Dichloro-1*H*-indol-1-yl)butyl)isoxazole-3-carboxylate (10a). To a stirred solution of **9a** (90 mg, 0.33 mmol) in DMF (3 mL) were added 5,6-dichloro-1*H*-indole (56 mg, 0.30 mmol) and Cs_2CO_3 (217 mg, 0.66 mmol) at room temperature. The resulting mixture was heated at 80 °C overnight. The reaction was quenched with a sat. NH_4Cl aqueous solution (5 mL) and extracted with EtOAc (10 mL × 3). The combined organic layers were washed with brine (30 mL), dried over Na_2SO_4, and concentrated under vacuum. The crude product was purified by flash chromatography (0 – 30% EtOAc/hexane) to afford **10a** as a colorless oil (90 mg, 80%). ^{1}H NMR (400 MHz, $CDCl_3$) δ 7.68 (s, 1H), 7.39 (s, 1H), 7.08 (d, *J* = 3.2 Hz, 1H), 6.42 (dd, *J* = 3.1, 0.7 Hz, 1H), 6.35 (s, 1H), 4.42 (q, *J* = 7.1 Hz, 2H), 4.09 (t, *J* = 6.9 Hz, 2H), 2.80 (t, *J* = 7.4 Hz, 2H), 1.92 – 1.85 (m, 2H), 1.77 – 1.65 (m, 2H), 1.41 (t, *J* = 7.1 Hz, 3H). ^{13}C NMR (101 MHz, $CDCl_3$) δ 174.5, 160.2, 156.6, 134.9, 129.7, 128.3, 125.7, 123.6, 122.1, 110.9, 101.9, 101.3, 62.3, 46.3, 29.5, 26.4, 25.0, 14.3.

Ethyl 5-(4-(6-Chloro-3,4-dihydroquinolin-1(2*H*)-yl)butyl)isoxazole-3-carboxylate (10b). To a stirred solution of **9b** (130 mg, 0.62 mmol) and **14a** (104 mg, 0.62 mmol) in EtOH/AcOH (5 mL/0.5 mL) was added $NaBH(OAc)_3$ (263 mg, 1.24 mmol) at room temperature. Then the resulting mixture was stirred at the same temperature overnight. The reaction was quenched with saturated aqueous $NaHCO_3$ solution (5 mL), and the mixture was extracted with DCM (10 mL × 3). The combined organic layers were washed with

brine, dried over Na_2SO_4, and concentrated under vacuum. The crude product was purified by flash chromatography (0 – 20% EtOAc/hexane) to afford **11b** as a colorless oil (130 mg, 58%). ^{1}H NMR (400 MHz, $CDCl_3$) δ 6.95 (dd, *J* = 8.7, 2.6 Hz, 1H), 6.88 (d, *J* = 2.6 Hz, 1H), 6.42 (d, *J* = 8.0 Hz, 1H), 6.41 (s, 1H), 4.43 (q, *J* = 7.1 Hz, 2H), 3.29 – 3.12 (m, 4H), 2.84 (t, *J* = 7.3 Hz, 2H), 2.69 (t, *J* = 6.3 Hz, 2H), 1.94 – 1.88 (m, 2H), 1.80 – 1.72 (m, 2H), 1.67 – 1.60 (m, 2H), 1.41 (t, *J* = 7.1 Hz, 3H). ^{13}C NMR (101 MHz, $CDCl_3$) δ 175.1, 160.2, 156.5, 143.8, 128.8, 126.8, 124.1, 120.1, 111.5, 101.7, 62.2, 51.1, 49.5, 28.1, 26.7, 25.7, 25.2, 22.1, 14.2.

Ethyl 5-(4-(6-Chloro-4,4-dimethyl-3,4-dihydroquinolin-1(2*H*)-yl)butyl)isoxazole-3-carboxylate (10c) was synthesized from **9b** (130 mg, 0.62 mmol) and **14b** (121 mg, 0.62 mmol) using a procedure similar to that described for the synthesis of **10b** and was obtained as a colorless oil (100 mg, 42%). ^{1}H NMR (400 MHz, $CDCl_3$) δ 7.10 (d, *J* = 2.6 Hz, 1H), 6.96 (dd, *J* = 8.8, 2.6 Hz, 1H), 6.42 (d, *J* = 9.5 Hz, 1H), 6.41 (s, 1H), 4.43 (q, *J* = 7.1 Hz, 2H), 3.32 – 3.19 (m, 4H), 2.85 (t, *J* = 7.4 Hz, 2H), 1.80 – 1.64 (m, 6H), 1.41 (t, *J* = 7.1 Hz, 3H), 1.25 (s, 6H). ^{13}C NMR (101 MHz, $CDCl_3$) δ 175.1, 160.3, 156.5, 142.5, 132.9, 126.6, 126.1, 120.3, 111.7, 101.8, 62.2, 51.3, 45.9, 36.8, 32.3, 30.6 (2C), 26.8, 25.6, 25.3, 14.3.

Ethyl 5-(4-(2,8-Dichloro-10,11-dihydro-5*H*-dibenz[*b*,*f*]azepin-5-yl)butyl)isoxazole-3-carboxylate (10d) was synthesized from **18** (100 mg, 0.30 mmol) and ethyl 2-chloro-2-(hydroxyimino)acetate (135 mg, 0.90 mmol) following ***General Procedure B*** and was obtained as a light-yellow oil (100 mg, 67%). ^{1}H NMR (400 MHz, $CDCl_3$) δ 7.09 − 7.08 (m, 4H), 6.96 − 6.93 (m, 2H), 6.31 (s, 1H), 4.43 (q, *J* = 7.1 Hz, 2H), 3.67 (t, *J* = 6.6 Hz, 2H), 3.10 (s, 4H), 2.74 (t, *J* = 7.4 Hz, 2H), 1.76 − 1.59 (m, 4H), 1.41 (t, *J* = 7.1 Hz, 3H).

5-(4-(5,6-Dichloro-1*H*-indol-1-yl)butyl)-*N*-hydroxyisoxazole-3-carboxamide (11a)

was synthesized from **10a** (90 mg, 0.24 mmol) following ***General Procedure C*** and was obtained as an off-white powder (35 mg, 39%). ^{1}H NMR (400 MHz, DMSO-d_6) δ 11.43 (s, 1H), 9.32 (d, J = 1.6 Hz, 1H), 7.89 (s, 1H), 7.79 (s, 1H), 7.51 (d, J = 3.1 Hz, 1H), 6.51 (s, 1H), 6.46 (d, J = 3.1 Hz, 1H), 4.22 (t, J = 7.0 Hz, 2H), 2.82 (t, J = 7.5 Hz, 2H), 1.65 – 1.75 (m, 2H), 1.65 – 1.54 (m, 2H). ^{13}C NMR (101 MHz, DMSO-d_6) δ 174.3, 157.4, 156.3, 134.7, 131.3, 127.9, 123.5, 121.5, 121.4, 111.7, 100.6, 100.5, 45.2, 29.14, 25.27, 24.12. ESI HRMS calc. for $C_{16}H_{16}N_3O_3Cl_2$: $[M+H]^+$, m/z 368.0563; found: 368.0555.

5-(4-(6-Chloro-3,4-dihydroquinolin-1(2*H*)-yl)butyl)-*N*-hydroxyisoxazole-3-carboxamide (11b) was synthesized from **10b** (130 mg, 0.36 mmol) following ***General Procedure C*** and was obtained as an off-white powder (100 mg, 79%). ^{1}H NMR (400 MHz, DMSO-d_6) δ 11.43 (s, 1H), 6.93 (dd, J = 8.7, 2.6 Hz, 1H), 6.88 (d, J = 2.7 Hz, 1H), 6.55 (s, 1H), 6.53 (d, J = 8.8 Hz, 1H), 3.29 – 3.16 (m, 4H), 2.84 (t, J = 7.4 Hz, 2H), 2.65 (t, J = 6.3 Hz, 2H), 1.86 – 1.77 (m, 2H), 1.69 – 1.64 (m, 2H), 1.57 – 1.50 (m, 2H). ^{13}C NMR (101 MHz, DMSO-d_6) δ 174.5, 157.4, 156.3, 143.8, 128.1, 126.3, 123.8, 118.1, 111.6, 100.5, 50.0, 48.5, 27.4, 25.7, 24.7, 24.4, 21.3. ESI HRMS calc. for $C_{17}H_{21}N_3O_3Cl$: $[M+H]^+$, m/z 350.1266; found: 350.1256.

5-(4-(6-Chloro-4,4-dimethyl-3,4-dihydroquinolin-1(2*H*)-yl)butyl)-*N*-hydroxyisoxazole-3-carboxamide (11c) was synthesized from **10c** (100 mg, 0.28 mmol) following ***General Procedure C*** and was obtained as an off-white powder (100 mg, 94%).^{1}H NMR (400 MHz, DMSO-d_6) δ 11.43 (s, 1H), 7.07 (d, J = 2.7 Hz, 1H), 6.94 (dd, J = 8.7, 2.6 Hz, 1H), 6.55 (s, 1H), 6.54 (d, J = 9.0 Hz, 1H), 3.28 – 3.21 (m, 4H), 2.84 (t, J = 7.3 Hz, 2H), 1.71 – 1.46 (m, 6H), 1.19 (s, 6H). ^{13}C NMR (101 MHz, DMSO-d_6) δ 174.5, 163.0, 157.4, 142.5, 132.5, 126.2, 125.3, 118.4, 111.9, 100.5, 50.2, 44.7, 40.2, 39.9, 39.7, 39.5, 39.3,

39.1, 38.9, 36.0, 31.8, 30.2 (2C), 25.6, 24.6, 24.5.ESI HRMS calc. for $C_{19}H_{24}N_3O_3Cl$: $[M+H]^+$, *m/z* 378.1579; found: 378.1576.

5-(4-(2,8-Dichloro-10,11-dihydro-5*H*-dibenz[*b*,*f*]azepin-5-yl)butyl)-*N*-hydroxyisoxazole-3-carboxamide (11d) was synthesized from **10d** (100 mg, 0.20 mmol) following ***General Procedure C*** and was obtained as a white powder (30 mg, 34%). ^{1}H NMR (400 MHz, $CDCl_3$) δ 7.09 − 7.07 (m, 4H), 6.95 − 6.92 (m, 2H), 6.37 (s, 1H), 3.66 (t, *J* = 6.5 Hz, 2H), 3.09 (s, 4H), 2.72 (t, *J* = 7.4 Hz, 2H), 1.76 − 1.68 (m, 2H), 1.63 − 1.57 (m, 2H); ^{13}C NMR (101 MHz, $CDCl_3$) δ 175.2, 156.0, 154.0, 146.3 (2C), 135.7 (2C), 129.7 (2C), 127.9 (2C), 126.4 (2C), 121.2 (2C), 100.7, 50.0, 31.7 (2C), 26.8, 26.7, 24.8. ESI HRMS calc. for $C_{22}H_{22}Cl_2N_3O_3$: $[M+H]^+$, *m/z* 446.1033; found: 446.1030.

3-Chloro-*N*-(4-chlorophenyl)propanamide (13a). To a round bottom flask charged with 4-chloroaniline (**12**, 5.0 g, 39.4 mmol) in acetone (50 mL) was added 3-chloropropanoyl chloride (1.9 mL, 19.7 mmol) at room temperature. The resulting mixture was allowed to stir for 1 h under reflux condition. The mixture was cooled to room temperature, quenched with 2N HCl (30 mL), and extracted with EtOAc (25 mL × 3). The combined organic layers were washed with brine (20 mL), dried over Na_2SO_4, and concentrated under vacuum. **13a** was obtained as an off-white powder (4.6 g, 54%) and used directly in the next step without further purification. ^{1}H NMR (400 MHz, $CDCl_3$) δ 7.56 (br s, 1H), 7.46 (d, *J* = 8.7 Hz, 2H), 7.28 (d, *J* = 8.8 Hz, 2H), 3.87 (t, *J* = 6.3 Hz, 2H), 2.81 (t, *J* = 6.3 Hz, 2H). ^{13}C NMR (101 MHz, $CDCl_3$) δ 167.9, 136.0, 129.8, 129.1 (2C), 121.4 (2C), 40.4, 39.8.

***N*-(4-Chlorophenyl)-3-methylbut-2-enamide (13b)**. To a round bottom flask charged with 4-chloroaniline (**12**, 1.27 g, 10.0 mmol) in $CHCl_3$ (20 mL) was added 3,3-dimethylacryloyl chloride (1.18 g, 10.0 mmol). The resulting mixture was heated to reflux

for 2 h. The mixture was cooled to room temperature and quenched with 2N HCl (20 mL), and then extracted with EtOAc (20 mL × 3). The combined organic layers were washed with brine (20 mL), dried over Na_2SO_4, and concentrated under vacuum. The crude product was purified by flash chromatography (0 – 80% EtOAc/hexane) to afford **13b** as a white powder (1.00 g, 48%). ^{1}H NMR (400 MHz, $CDCl_3$) δ 7.54 (br s, 1H), 7.47 (d, *J* = 8.1 Hz, 2H), 7.22 (d, *J* = 8.8 Hz, 2H), 5.70 (s, 1H), 2.19 (s, 3H), 1.86 (s, 3H). ^{13}C NMR (101 MHz, $CDCl_3$) δ 165.2, 154.0, 136.8, 128.8 (4C), 121.0, 118.4, 27.3, 20.0.

6-Chloro-1,2,3,4-tetrahydroquinoline (14a). (i) In a three-necked flask charged with **13a** (4.6 g, 21.1 mmol) under an argon atmosphere was added $AlCl_3$ (5.47 g, 42.2 mmol) at 140 °C. The resulting mixture was stirred at the same temperature for 12 h. Then the reaction was cautiously quenched with 1 N HCl (20 mL) at 0 °C, and the mixture was extracted with EtOAc (30 mL × 3). The combined organic extracts were washed with brine (20 mL), dried over Na_2SO_4, and concentrated under vacuum. The crude product was purified by flash chromatography (0 – 80% EtOAc/hexane) to afford the lactam intermediate as a white powder (3.1 g, 17.1 mmol). (ii) To a stirred solution of $LiAlH_4$ (1.95 g, 51.4 mmol) in THF (30 mL) were added dropwise a solution of the lactam intermediate (3.1 g, 17.1 mmol) in THF (20 mL) at 0 °C. The resulting mixture was stirred at the same temperature for 20 min and then heated at reflux for an additional 1 h. The reaction was subsequently quenched with water (2.0 mL), 5 N NaOH (2.0 mL), and water (10 mL). The resulting precipitate was filtered off and washed with EtOAc (20 mL × 3). The filtrate was washed with brine (20 mL), dried over Na_2SO_4, and concentrated under vacuum. **14a** was obtained as a colorless oil (2.43 g, 70% over two steps) and used directly in the next step without further purification. ^{1}H NMR (400 MHz, $CDCl_3$) δ 6.93 – 6.86 (m, 2H), 6.38 (d, *J* = 8.0 Hz, 1H),

3.77 (br s, 1H), 3.33 – 3.15 (m, 2H), 2.72 (t, J = 6.4 Hz, 2H), 1.94 – 1.88 (m, 2H). ^{13}C NMR (101 MHz, $CDCl_3$) δ 143.2, 128.8, 126.3, 122.7, 120.9, 114.9, 41.7, 26.7, 21.6.

6-Chloro-4,4-dimethyl-1,2,3,4-tetrahydroquinoline (14b). (i) To a round bottom flask charged with **13b** (1.0 g, 4.78 mmol) in Toluene (15 mL) was added $AlCl_3$ (2.50 g, 19.1 mmol) at room temperature. The resulting mixture was heated at 80 °C for 2 h. Then the reaction was cautiously quenched with 1 N HCl (10 mL) at 0 °C, and the mixture was extracted with EtOAc (15 mL × 3). The combined organic layers were washed with brine (20 mL), dried over Na_2SO_4, and concentrated under vacuum. The crude product was purified by flash chromatography (0 – 80% EtOAc/hexane) to afford the lactam intermediate as a brown powder (640 mg, 64%); (ii) To a stirred solution of $LiAlH_4$ (250 mg, 6.60 mmol) in THF (10 mL) was dropwise added the lactam intermediate (460 mg, 2.20 mmol) in THF (20 mL) at 0 °C. The resulting mixture was stirred at the same temperature for 20 min and then heated to reflux condition for an additional 1 h. The reaction was subsequently quenched with water (0.5 mL), 5 N NaOH (0.5 mL), and water (2.5 mL). The resulting precipitate was filtered off and washed with EtOAc (20 mL × 3). The filtrate was washed with brine (20 mL), dried over Na_2SO_4, and concentrated under vacuum. The crude product was purified by flash chromatography (0 – 20% EtOAc/hexane) to afford compound **14b** as a colorless oil (370 mg, 86%). ^{1}H NMR (400 MHz, DMSO-d_6) δ 7.05 (d, J = 2.5 Hz, 1H), 6.83 (dd, J = 8.6, 2.5 Hz, 1H), 6.44 (d, J = 8.6 Hz, 1H), 5.91 (br s, 1H), 3.21 – 3.12 (m, 2H), 1.61 – 1.53 (m, 2H), 1.20 (s, 6H). ^{13}C NMR (101 MHz, DMSO-d_6) δ 143.1, 130.5, 125.9, 125.3, 118.3, 114.8, 37.0, 36.0, 31.5, 30.3 (2C).

2,8-Dichloro-10,11-dihydro-5*H*-dibenz[*b,f*]azepine (16). To a stirred solution of 10,11-

dihydro-5*H*-dibenz[*b,f*]azepine (**15**, 500 mg, 2.56 mmol) in $CHCl_3$ (75 mL) was added at room temperature pre-dried silica gel (10 g, 2 g per mmol of NCS). The mixture was stirred gently, and the reaction vessel covered with foil to exclude light. NCS (685 mg, 5.12 mmol) was then added portion wise over 1 h at room temperature. The mixture was stirred at the same temperature overnight. After completion of the reaction, excess silica gel was removed by vacuum filtration. The filtrate was washed with water and brine, dried over Na_2SO_4, and concentrated under reduced pressure. The crude product was purified by flash chromatography using (0 – 10% EtOAc/hexane) to afford **16** as a white solid (500 mg, 74%). ^{1}H NMR (400 MHz, $CDCl_3$) δ 7.04 − 7.02 (m, 4H), 6.65 (d, J = 6.2 Hz, 2H), 5.93 (s, 1H), 3.02 (s, 4H).

2,8-Dichloro-5-(hex-5-yn-1-yl)-10,11-dihydro-5*H*-dibenzo[*b,f*]azepine (18). (i) To a stirred solution of **16** (300 mg, 1.15 mmol) in DMF (5 mL) was slowly added NaH (60%, 140 mg, 3.45 mmol). The mixture was stirred at room temperature for 15 min, followed by dropwise addition of 1,4-dibromobutane (364 mg, 1.7 mmol). The mixture was stirred at room temperature for 1 h. After completion of the reaction, 1 N HCl aqueous solution was added to adjust the pH to 6~7. Then the solution was extracted with EtOAc (10 mL × 3). The combined organic layers were washed with brine, dried over Na_2SO_4, and concentrated under reduced pressure. The crude product was purified by flash chromatography (0-5% EtOAc/hexane) to afford **17** as a colorless oil (200 mg, 43%). (ii) To a stirred solution of **17** (200 mg, 0.5 mmol) in xylene/DMF (2/2 mL) was added sodium acetylide suspension (0.2 mL, 18 wt. % slurry in xylene) under an argon atmosphere at room temperature. Then the mixture was stirred at 40 °C overnight. After completion, the reaction solution was quenched with water (10 mL), and the mixture was extracted with EtOAc (10 mL × 3). The

combined organic layers were washed with brine, dried over Na_2SO_4, and concentrated under reduced pressure. The crude product was purified by flash chromatography (0 − 5% EtOAc/hexane) to afford **18** (100 mg, 25%) as a colorless oil. ^{1}H NMR (400 MHz, $CDCl_3$) δ 7.09 − 7.07 (m, 4H), 6.97 (d, *J* = 9.0 Hz, 2H), 3.67 (t, *J* = 6.8 Hz, 2H), 3.10 (s, 4H), 2.14 (td, *J* = 7.0, 2.6 Hz, 2H), 1.89 (t, *J* = 2.6 Hz, 1H), 1.67− 1.64 (m, 2H), 1.55 − 1.51 (m, 2H).

Ethyl 5-(3-((3,4-Dichlorophenyl)amino)propyl)isoxazole-3-carboxylate (19a) was synthesized from **9c** (464 mg, 2.85 mmol) and 3,4-dichlorophenol (850 mg, 3.41 mmol) using a procedure similar to that described for the synthesis of **10a** and was obtained as a colorless oil (490 mg, 80%). ^{1}H NMR (400 MHz, $CDCl_3$) δ 7.28 (d, *J* = 8.9 Hz, 1H), 6.94 (d, *J* = 2.8 Hz, 1H), 6.71 (dd, *J* = 8.9, 2.9 Hz, 1H), 6.43 (s, 1H), 4.41 (q, *J* = 7.1 Hz, 2H), 3.96 (t, *J* = 5.9 Hz, 2H), 3.00 (t, *J* = 7.5 Hz, 2H), 2.26 – 2.08 (m, 2H), 1.38 (t, *J* = 7.1 Hz, 3H). ^{13}C NMR (101 MHz, $CDCl_3$) δ 174.3, 160.1, 157.7, 156.5, 132.9, 130.8, 124.2, 116.4, 114.5, 102.0, 66.9, 62.2, 27.0, 23.4, 14.2.

Ethyl 5-(4-(3,4-Dichlorophenyl)butyl)isoxazole-3-carboxylate (19b) was synthesized from **25** (18 mg, 0.1 mmol) following **General Procedure B** and was obtained as a colorless oil (20 mg, 58%). ^{1}H NMR (400 MHz, $CDCl_3$) δ 7.34 (d, *J* = 8.2 Hz, 1H), 7.25 (d, *J* = 2.0 Hz, 1H), 6.99 (dd, *J* = 8.2, 2.0 Hz, 1H), 6.40 (s, 1H), 4.55 – 4.46 (m, 2H), 2.83 (t, *J* = 7.3 Hz, 2H), 2.61 (t, *J* = 7.4 Hz, 2H), 1.78 – 1.64 (m, 4H).

5-(3-((3,4-Dichlorophenyl)amino)propyl)-*N*-hydroxyisoxazole-3-carboxamide (20a) was synthesized from **19a** (160 mg, 0.47 mmol) following ***General Procedure C*** and was obtained as a white powder (65 mg, 40%). ^{1}H NMR (400 MHz, DMSO-d_6) δ 11.45 (s, 1H), 9.33 (s, 1H), 7.51 (d, *J* = 8.9 Hz, 1H), 7.23 (d, *J* = 2.9 Hz, 1H), 6.96 (dd, *J* = 8.9, 2.9 Hz, 1H), 6.60 (s, 1H), 4.06 (t, *J* = 6.1 Hz, 2H), 2.96 (t, *J* = 7.5 Hz, 2H), 2.15 – 2.03 (m, 2H).

^{13}C NMR (101 MHz, DMSO-d_6) δ 173.8, 157.9, 157.5, 156.3, 131.6, 131.0, 122.4, 116.4, 115.5, 100.7, 67.2, 40.2, 39.9, 39.7, 39.5, 39.3, 39.1, 38.9, 26.4, 22.6. ESI HRMS calc. for $C_{13}H_{13}Cl_2N_2O_4$: $[M+H]^+$, *m/z* 331.0247; found: 331.0244.

5-(4-(3,4-Dichlorophenyl)butyl)-*N*-hydroxyisoxazole-3-carboxamide (20b) was synthesized from **19b** (50 mg, 0.15 mmol) following ***General Procedure C*** and was obtained as an off-white powder (15 mg, 30%). ^{1}H NMR (400 MHz, $CDCl_3$) δ 7.34 (d, *J* = 8.1 Hz, 1H), 7.24 (s, 1H), 6.98 (d, *J* = 7.7 Hz, 1H), 6.45 (s, 1H), 2.82 (t, *J* = 7.2 Hz, 2H), 2.60 (t, *J* = 7.2 Hz, 2H), 1.78 – 1.61 (m, 4H). ^{13}C NMR (101 MHz, $CDCl_3$) δ 175.2, 169.0, 156.2, 141.9, 132.3, 130.3, 130.3, 129.9, 127.8, 100.8, 34.6, 30.3, 26.8, 26.5. ESI HRMS calc. for $C_{14}H_{15}Cl_2N_2O_3$: $[M+H]^+$, *m/z* 329.0454; found: 329.0456.

3,4-Dichloro-*N*-(4-(hydroxycarbamoyl)benzyl)benzamide (20c). (i) To a stirred suspension of 3,4-dichlorobenzaldehyde (**26**, 1.04 g, 6.0 mmol) in water (20 mL) were added $NH_2OH{\cdot}HCl$ (0.42 g, 6.0 mmol) and K_2CO_3 (0.83 g, 6.0 mmol), followed by addition of $Cu(OAc)_2$ (20 mg, 0.12 mmol). The reaction mixture was heated to reflux for 6 h. After completion of the reaction, the solution was extracted with EtOAc (20 mL × 3). The combined organic layers were washed with brine, dried over Na_2SO_4, and concentrated under vacuum. The crude product was washed with Et_2O to afford amide intermediate **27** as a white powder (0.80 g, 70%). (ii) To a suspension of 3,4-dichlorobenzamide (**27**, 0.80 g, 4.25 mmol) and methyl 4-formylbenzoate (232 mg, 1.41 mmol) in toluene (10 mL) was added TFA (325 μL, 4.25mmol) and triethylsilane (677 μL, 4.25 mmol) at room temperature. The resulting mixture was heated to reflux overnight. After completion of the reaction, the solution was extracted with EtOAc (20 mL × 3). The combined organic layers were washed with brine, dried over Na_2SO_4, and concentrated under vacuum. The crude

product **19c** containing excess dichlorobenzamide (~800 mg) was advanced in the next step without further purification. (iii) Compound **20c** was synthesized from the crude compound **19c** (~800 mg) following ***General Procedure C*** and was obtained as an off-white powder (150 mg, 31% over two steps). ^{1}H NMR (500 MHz, DMSO-d_6) δ 11.17 (s, 1H), 9.27 (t, J = 6.0 Hz, 1H), 8.99 (s, 1H), 8.13 (d, J = 2.1 Hz, 1H), 7.87 (dd, J = 8.4, 2.1 Hz, 1H), 7.78 (d, J = 8.4 Hz, 1H), 7.71 (d, J = 8.0 Hz, 2H), 7.38 (d, J = 8.0 Hz, 2H), 4.51 (d, J = 5.9 Hz, 2H). ^{13}C NMR (126 MHz, DMSO-d_6) δ 164.0, 164.0, 142.4, 134.5, 134.1, 131.4, 131.3, 130.8, 129.2, 127.6, 127.2 (2C), 126.9 (2C), 42.6. ESI HRMS calc. for $C_{15}H_{13}Cl_2N_2O_3$: $[M+H]^+$, m/z 339.0298; found: 339.0306.

4-(3-Bromopropyl)-1,2-dichlorobenzene (22). (i) A suspension of $LiAlH_4$ (262 mg, 6.9 mmol) in THF (23 mmol, 0.3 M solution) was prepared in an ice bath and under an argon atmosphere. To this suspension was added dropwise a THF solution (8 mL) of 3,4-dichlorocinnamic acid (**21**, 500 mg, 2.3 mmol). After the addition of the substrate solution, the resulting mixture was left to warm to room temperature while stirring. Then it was heated to reflux for 5 h. The reaction was quenched with water (0.3 mL), 5N NaOH (0.3 mL), and water (1.5 mL), the precipitate was filtered off, and the filtrate was extracted with EtOAc (10 mL × 3). The organic layers were washed with brine, dried over Na_2SO_4, and concentrated under vacuum. The crude product was purified by flash chromatography (0 – 50% EtOAc/hexane) to afford the intermediate alcohol as a colorless oil (80 mg, 17%). (ii) To a stirred solution of the intermediate (80 mg, 0.40 mmol) in DCM (5 mL) were added CBr_4 (194 mg, 0.6 mmol) and Ph_3P (160 mg, 0.6 mmol) at 0 °C. Then the resulting mixture was stirred at room temperature for 1 h. The reaction was quenched with water (5 mL), extracted with DCM (10 mL × 3). The combined organic extracts were washed with brine

(30 mL), dried over Na_2SO_4, and concentrated under vacuum. The crude product was purified by flash chromatography (0 – 20% EtOAc/hexane) to afford **22** as a colorless oil (70 mg, 65%). ^{1}H NMR (400 MHz, $CDCl_3$) δ 7.36 (d, *J* = 8.2 Hz, 1H), 7.29 (d, *J* = 2.0 Hz, 1H), 7.04 (dd, *J* = 8.2, 2.1 Hz, 1H), 3.38 (t, *J* = 6.4 Hz, 2H), 2.79 – 2.70 (m, 2H), 2.19 – 2.08 (m, 2H). ^{13}C NMR (101 MHz, $CDCl_3$) δ 140.8, 132.4, 130.5, 130.4, 130.2, 128.0, 33.7, 33.1, 32.5.

4-(3,4-Dichlorophenyl)butanenitrile (23). To a solution of **22** (70 mg, 0.26 mmol) in DMSO (3 mL) were added NaCN (115 mg, 2.36 mmol) at room temperature. Then the resulting mixture was heated at 100 °C for 1 h. The mixture was diluted with water (5 mL) and extracted with EtOAc (10 mL × 3). The combined organic extracts were washed with aqueous $FeSO_4$ solution (10 mL) and brine (10 mL), dried over Na_2SO_4, and concentrated under vacuum. Compound **23** was obtained as a yellow oil (40 mg, 72%) and used directly into the next step without further purification. ^{1}H NMR (400 MHz, $CDCl_3$) δ 7.37 (dd, *J* = 8.2, 0.8 Hz, 1H), 7.28 (d, *J* = 1.2 Hz, 1H), 7.03 (dd, *J* = 8.2, 1.5 Hz, 1H), 2.75 (t, *J* = 7.5 Hz, 2H), 2.34 (t, *J* = 7.0 Hz, 2H), 1.96 (p, *J* = 7.1 Hz, 2H). ^{13}C NMR (101 MHz, $CDCl_3$) δ 140.0, 132.6, 130.6, 130.4 (2C, overlapping), 127.9, 119.1, 33.5, 26.6, 16.4.

4-(3,4-Dichlorophenyl)butan-1-ol (24). (i) To a stirred solution of **23** (40 mg, 0.19 mmol) in EtOH (1 mL) was added 50% *w/v* aq. NaOH (1 mL) at room temperature. The resulting mixture was heated at 80 °C for 3 h. Then the mixture was diluted with water (5 mL) and extracted with EtOAc (10 mL × 3). The aqueous layer was separated and acidified with 2N HCl to pH = 3–4, then extracted with EtOAc (10 mL × 3). The combined organic layers were washed with brine (30 mL), dried over Na_2SO_4, and concentrated under vacuum. The crude carboxylic acid product was obtained as a pink solid (40 mg, 90%) and used directly

in the next step without further purification. (ii) To a stirred solution of the carboxylic acid (40 mg, 0.17 mmol) in THF (3 mL) was added $BF_3 \cdot THF$ (1 M in THF, 0.34 mL) at 0 °C over 5 min. The resulting mixture was allowed to warm to room temperature overnight. The reaction was quenched with 1N NaOH, and the mixture was extracted with EtOAc (10 mL × 3). The combined organic layers were washed with water (30 mL) and brine (30 mL), dried over Na_2SO_4, and concentrated under vacuum. **24** was obtained as a colorless oil (40 mg, 98%) and used directly in the next step without further purification. ^{1}H NMR (400 MHz, $CDCl_3$) δ 7.33 (d, *J* = 8.2 Hz, 1H), 7.27 (d, *J* = 1.8 Hz, 1H), 7.01 (dd, *J* = 8.2, 1.8 Hz, 1H), 3.66 (t, *J* = 6.3 Hz, 2H), 2.60 (t, *J* = 7.5 Hz, 2H), 1.74 – 1.64 (m, 2H), 1.62 – 1.55 (m, 2H), 1.53 (br s, 1H). ^{13}C NMR (101 MHz, $CDCl_3$) δ 142.6, 132.2, 130.3, 130.2, 129.7, 127.9, 62.6, 34.8, 32.1, 27.3.

1,2-Dichloro-4-(hex-5-yn-1-yl)benzene (25). (i) To a stirred solution of **24** (40 mg, 0.18 mmol) in DCM (3 mL) were added CBr_4 (90 mg, 0.27 mmol) and Ph_3P (70 mg, 0.27 mmol) at 0 °C. Then the resulting mixture was stirred at room temperature for 1 h. The reaction was quenched with water (5 mL) and extracted with DCM (10 mL × 3). The combined organic layers were washed with brine (30 mL), dried over Na_2SO_4, and concentrated under vacuum. The crude product was purified by flash chromatography (0 – 20% EtOAc/hexane) to afford the intermediate bromide as a colorless oil (20 mg, 40%). (ii) To a stirred solution of the bromide (20 mg, 0.07 mmol) in DMF (2 mL) was added sodium acetylide suspension (18 wt. % slurry in xylene, 0.03 mL) under an argon atmosphere. The resulting mixture was stirred at 40 °C overnight. The reaction was quenched with water (5 mL), extracted with EtOAc (10 mL × 3). The combined organic layers were washed with brine (30 mL), dried over Na_2SO_4, and concentrated under vacuum. **25** was obtained as a

colorless oil (18 mg, 98%) and used directly in the next step without further purification. ^{1}H NMR (400 MHz, $CDCl_3$) δ 7.33 (d, *J* = 8.2 Hz, 1H), 7.28 – 7.25 (m, 1H), 7.01 (dd, *J* = 8.2, 2.0 Hz, 1H), 2.59 (t, *J* = 7.7 Hz, 2H), 2.22 (td, *J* = 7.0, 2.6 Hz, 2H), 1.95 (t, *J* = 2.6 Hz, 1H), 1.74 – 1.70 (m, 2H), 1.58 – 1.51 (m, 2H). ^{13}C NMR (101 MHz, $CDCl_3$) δ 142.4, 132.2, 130.3, 130.2, 129.7, 127.9, 84.0, 68.6, 34.5, 30.0, 27.8, 18.2.

HDAC 1 and 6 enzymatic assay procedure. HDAC inhibition assays in Table 1 were performed by the Reaction Biology Corporation (Malvern, PA) using human full-length recombinant HDAC1 and 6, isolated from a baculovirus expression system in Sf9 cells. An acetylated, fluorogenic peptide derived from residues 379-382 of p53 (RHKKAc, 50 μM) was used as the substrate in the assays. The reaction buffer contained: 50 mM Tris·HCl pH 8.0, 137 mM NaCl, 2.7 mM KCl, 1 mM $MgCl_2$, 1 mg/mL BSA, and a final concentration of 1% DMSO. The enzyme was added into wells of the reaction plate and stock solutions of compounds were distributed into the enzyme mixture by acoustic technology (Echo550 instrument; nanoliter range). The plates were spun down and pre-incubated for 5-10 min. The substrate was then delivered to all reaction wells to initiate the reaction, which was incubated for 2 h at 30 °C. After incubation, developer and trichostatin A (TSA) were added to quench the reaction and generate fluorescence. Kinetic measurements were then taken for 1.5 h at 15 min intervals to ensure that development was complete. Endpoint readings were taken for analysis after the development reached a plateau. Dose response curves were generated, and the IC_{50} value for each compound was extrapolated from the generated plots (10-point IC_{50} curves were generated using a 3-fold serial dilution pattern starting at 30 μM).

Expression and purification of HDACs1, 4-9, and 11. Large scale expression of human

HDACs was carried out in HEK293/T17 cells essentially as described previously.[92, 93] Briefly, transiently transfected cells were harvested three days post transfection and the cell pellets resuspended in a lysis buffer (50 mM Tris, 150 mM NaCl, 10 mM KCl, 2 mM $MgCl_2$, 10% glycerol, 0.2% NP-40, 2 Units/mL benzonase, pH 8) supplemented with a cocktail of protease inhibitors (Roche, Basel, Switzerland). Cells were lysed by sonication (30 W; 3 × 20 s) on ice and the cell lysate cleared by centrifugation at 40, 000 × *g* for 30 min at 4 °C. Recombinant fusion HDAC proteins were purified *via* Strep-Tactin affinity chromatography (IBA, Göttingen, Germany) with the elution buffer comprising 50 mM HEPES, 100 mM NaCl, 50 mM KCl, 10% glycerol, and 3 mM desthiobiotin, pH 7.5. Purified proteins were concentrated to 1 mg/mL, aliquoted, flash-frozen in liquid nitrogen and stored at -80 °C until further use.

Determination of inhibitory activity against HDACs1, 4-9, and 11. IC_{50} values in Table 2 were determined using a fluorescence-based assay with 10 μM Ac-GAK(Ac)-AMC (HDAC 1, 6) or 10 μM Boc-Lys(TFA)-AMC (HDAC 4, 5, 7, 8, 9, 11) as a substrate.[94] Briefly, individual HDACs were preincubated with dilution series of tested inhibitors (0 – 100 μM) in a 384-well plate in the total volume of 40 μL for 10 min at 37 °C in a reaction buffer comprising 50 mM HEPES, 140 mM NaCl, 10 mM KCl, 1 mM TCEP, 0.1% BSA, pH 7.4. Deacetylation reaction was started by the addition of 10 μL of a 10 μM substrate into the HDAC/inhibitor mixture. Following the 30 min incubation at 37 °C, the reaction was terminated by the addition of 25 μL of the trypsin solution (4 mg/mL). Fluorescence development by trypsin was carried out at 37 °C for 15 and 60 min for Ac-GAK(Ac)-AMC and Boc-Lys(TFA)-AMC substrate, respectively. Released aminomethylcoumarin was quantified using a CLARIOstar fluorimeter with the excitation and emission wavelengths

set to 365 nm and 440 nm, respectively. Non-linear regression analysis was employed to calculate IC_{50} values using the GraphPad Prism software (10-point IC_{50} curves were generated using a 3-fold serial dilution pattern starting at 100 μM). Reactions without the enzyme or the inhibitor were used to define 0% and 100% of the HDAC activity, respectively.

drHDAC6 expression and purification. The second catalytic domain of HDAC6 from *Danio rerio* (drHDAC6; amino acids 440 - 798) was expressed and purified essentially as described previousl.[88] Briefly, the synthetic gene encoding HDAC6 was recombined into a Gateway expression plasmid in frame with the TEV-cleavable His-MBP N-terminal tag. The fusion protein was expressed in *E. coli* BL21-Codon plus (DE3)-RIPL at 16 °C overnight. The purification protocol comprised the HisTrap HP affinity step (GE Healthcare, Chicago, IL, USA), removal of the tag by the TEV protease, affinity purification on an amylose resin (New England Biolabs, Ipswitch, MA, USA), ion-exchange chromatography on HiTrap Q sepharose (GE Healthcare), and size-exclusion chromatography on a HiLoad Superdex 75 pg column (GE Healthcare; mobile phase: 50 mM HEPES, 100 mM KCl, 5% glycerol, 1 mM TCEP, pH 7.5) as the final step. Purity of the final protein preparation was > 98% as determined by SDS-PAGE and purified drHDAC6-CD2 was concentrated to 10 mg/mL, aliquoted, flash-frozen in liquid nitrogen and stored at -80 °C until further use.

Crystallization and data collection. The drHDAC6 stock solution was mixed with 1/20 volume of the SS-208 solution (80 mM in DMSO), and the crystallization droplets were prepared by combining 1 μL of the complex solution with 1 μL of a reservoir solution containing 19% PEG 3350 (Sigma Aldrich), 0.2 M KSCN (Hampton research), 0.1 M Bis-

Tris (Sigma Aldrich) at pH 6.5. To bolster the nucleation step, droplets were streak-seeded using the seed stock prepared from crystals of the HDAC6/SAHA complex using a Crystal Crusher (Hampton Research). Crystals were grown by the hanging drop vapor diffusion method at 283 K. Diffraction quality crystals were vitrified in liquid nitrogen from the mother liquor supplemented with 20% (*v/v*) glycerol. The diffraction data were collected from a single crystal at 90 K using synchrotron radiation at the Bessy II beamline MX 14.2 (Berlin, Germany) equipped with the Pilatus 2M detector at an X-ray wavelength of 0.92 Å. Data processing was performed with the XDSAPP software package.[95]

Structure determination and refinement. The difference Fourier method was used to determine the structure of the drHDAC6-CD2/SS-208 complex using the drHDAC6/TSA complex (PDB code: 5EEK) without the inhibitor and water molecules as a starting model.[88] Iterative refinement and model building cycles were performed using Refmac 5.8. and Coot, respectively.[96, 97] Ligand topologies and coordinates were generated with AceDRG[98] and the inhibitor was fitted into the |Fo| − |Fc| electron density maps in the final stages of the refinement. Approximately 2,500 randomly selected reflections were kept aside for cross-validation (Rfree) during the refinement process. The final model was validated using the MolProbity server.[99] The data collection and structure refinement statistics are summarized in the Table S4.

Cell transfection, treatments, and BRET measurements. NanoBRET target engagement was performed against HDAC6 (CD2) and HDAC1 according to the manufacturer's protocol (Promega) in HEK293 cells (ATCC). Plasmid constructs encoding NanoLuc-HDAC6 (CD2) and HDAC1-NanoLuc encoded HDAC open reading frames matching previous work.[89] HDAC6 (CD2) encoded a GSSGAIA linker between Nanoluc

and HDAC6 (CD2), and HDAC1-NanoLuc encoded a SWTWEGNKWTWK linker between HDAC1 and NanoLuc. NanoBRET HDAC Tracer (Promega) was added to a final concentration of 250 nM and 1000 nM for HDAC6 (CD2) and HDAC1, respectively, immediately prior to test compound addition. Tracer concentrations were selected for each HDAC such that tracer occupancy did not impart a shift in observed compound IC_{50} value. Serially-diluted test compounds were then added to the cells and allowed to equilibrate for 2 h prior to BRET measurements. To measure BRET, NanoBRET NanoGlo Substrate- (Promega) and Extracellular NanoLuc inhibitor was added per the manufacturer's protocol, and filtered luminescence was measured on a GloMax Discover luminometer equipped with a 450 nm BP filter (donor) and 610 nm LP filter (acceptor), using a 0.5 s integration time. Milli-BRET units (mBU) are the BRET values × 1000. Competitive displacement data were then graphed with GraphPad Prism software using a 3-parameter curve fit with the following equation (Equation).

$$Y=Bottom + (Top-Bottom) / [1+10^{(X-LogIC_{50})}].$$

Mice. Experiments involving mice were performed in accordance with approved protocols by the Institutional Care and Use Committee (IACUC) at The George Washington University (Protocol A354). C57BL/6 mice were obtained from the Charles River Laboratories (Wilmington, Massachusetts, USA). All the *in vivo* studies performed used tumor cells passaged *in vivo* (mouse to mouse) a minimum of five times before the tumor challenge experiment. Once *in vivo* passaged cells were obtained, mice were injected subcutaneously with 1.0×10^6 melanoma cells suspended in 100 μL 1X phosphate buffered saline (PBS) (Corning, 21-040-CV). Treatment started once tumors were palpable or as indicated in particular experiments. Mice were treated intraperitoneally with SS-208 (25

mg/kg) or vehicle control depending on the randomly assigned treatment group (10 female mice per group, 4-6 weeks old). Control mice were injected with 100 μL 1× PBS as vehicle control. Mice were treated five days a week until tumors in the control group reached maximum size according to our IACUC protocol. Tumor volume was calculated using caliper measurements by the formula L × W2/2.

All animal studies were done with consideration for toxicity in relation to each individual agent and using a dose that was previously verified through *in vivo* testing. However, we routinely monitored for early signs of toxicity. Particular focus was given to mortality, body weight, and food consumption. At the end-point postmortem evaluation, using gross visual examination of organs, was done for each condition.

Cell culture. *In vivo* tumors: SM1 cells were originally obtained from the laboratory of Dr. A. Ribas at the University of California Los Angeles.[100] SM1 tumor cells were passaged *in vivo* directly from mouse to mouse for at least five passages. Tumors were grown and selected for optimal and consistent growth rate. When preparing cells for subcutaneous injection, mice with a tumor burden measuring approximately 7 mm × 7 mm were euthanized. Tumors were extracted and processed under sterile conditions. A cell count was used to adjust the cell concentration to 1.0×10^6 per 100 μL of PBS, indicative of the volume per mouse injection. These cells were immediately injected into the experimental mice, as described above. Cells in excess from the tumor processing were frozen in 90% Fetal Bovine Serum (FBS) (Serum Source, FB02-500HI) with 10% DMSO (Sigma-Aldrich, D2650) and stored in liquid nitrogen for future experiments.

HDACis for cellular studies. SS-208 was kept as a stock solution of 10 mg/mL and diluted with a buffer provided by the manufacturer to the concentration used for each particular

experiment. Nexturastat A (NextA) was provided by StarWise Therapeutics LLC. Tubastatin A (TubA, S8049) was purchased from Selleckchem. The pan-HDACi LBH589 (50-148-338) was purchased from Biotang Inc.

Cellular viability and apoptosis assays. Using ApoTox-Glo Triplex Assay® (Promega, G6321) viability and apoptosis were measured. SM1 cells were treated with individual HDACis along with the recommended assay controls. Pan-HDACi, LBH589 was also used as a control on all plates. Following the manufacturer's protocol, Viability/Cytotoxicity reagents were added, and fluorescence was measured at specific wavelengths – i.e., 400Ex/505Em (viability) and 485Ex/520Em (cytotoxicity). Next, the Caspase 3/7 reagent was added, and luminescence was measured at Lm578 (apoptosis). Measurements were collected using the SpectraMax 3i multi-mode microplate reader.

Cellular HDAC inhibition. Using HDAC-Glo I/II Assay® (Promega, G6420) Cells were plated at a density of 10,000 cells per/well overnight in a white, flat clear bottom 96 well plate. After 24 h, the plate was then treated with the compounds of interest (NextA, TubA, and SS-208) at the desired concentrations and incubated at 37 °C and 5% CO_2 for 1 h. After incubation with the compounds, the developer is added to the substrate, mixed, and added directly to the plate, following the manufactured protocol. Immediately after plating, the plate was read for an hour and 15 min with a reading done every 2 min, using the SpectraMax 3i multi-mode plate reader.

Flow cytometry. Tumor cells were immediately processed into single cell suspensions for analysis by flow cytometry. The first panel for flow cytometry was to analyze the expression of immune cell surface markers. These cells were stained with phycoerythrin (PE) conjugated antibodies in a 96-well format. Antibodies were purchased from BD

Biosciences (San Jose, California, USA), Biolegend (San Diego, California, USA), and eBioscience (San Diego, California, USA). Tumor cells were stained with anti-mouse CD274 (PD-L1) (BD Biosciences, 558091), anti-mouse CD 273 (PD-L2) (Biolegend, 107205), anti-mouse CD276 (B7-H3) (Biolegend, 124507), anti-mouse B7-H4 (Biolegend, 139405), anti-mouse Galactin-9 (Biolegend, 137903), anti-mouse CD252 (OX40-L), anti-mouse CD275 (ICOS-L) (eBioscience, 12-5985-81), anti-mouse MHC I (H-2Kb)(eBioscience, 12-5958-80), or anti-mouse MHC II (I-A/I-E) (eBioscience, 12-5321-81). After staining for 30 min at room temperature, cells were washed at least three times with 1× PBS and resuspended in FACS buffer.

The second panel for flow cytometry was designed to measure the activity and infiltration of Natural Killer (NK) and T-cells. The following antibodies were used: PerCP/Cy5.5 anti-mouse CD3 (T-cells) (Biolegend, 100218), Alexa Fluor 488 anti-mouse CD4 (CD4+ T cells) (Biolegend, 100423), PE/Cy7 anti-mouse CD8a (CD8+ T cells) (Biolegend, 100766), APC/Fire 750 anti-mouse CD49b (NK cells) (Biolegend, 108922), Brilliant Violet 421 anti-mouse CD25 (T-cell activation) (Biolegend, 102034), and Brilliant Violet 785 anti-mouse CD45.2 (T-cell activation) (Biolegend, 109839). Finally, the third flow cytometry panel measured the activity and infiltration of myeloid cells using the following markers: Brilliant Violet 421 anti-mouse/human C11b (Macrophage) (Biolegend, 101236), APC anti-mouse CD80 (M1) (Biolegend, 104714), PE/Cy7 anti-mouse CD206 MMR (M2) (Biolegend, 141720), Brilliant Violet 630 anti-mouse CD11c (mDC) (Biolegend, 117339), APC/Fire 750 anti-mouse CD45.2 (MDSC) (Biolegend, 109852), PE anti-mouse CD123 [IL-3 receptor (IL-3Rα)] (Biolegend, 106005), Brilliant Violet 603 anti-mouse Ly-6G/Ly-6C (MDSC) (Biolegend, 108440), FITC anti-mouse H 2 (M2) (Biolegend, 125508),

and Brilliant Violet 785 anti-mouse F4/80 (Macrophage) (Biolegend, 123141). After staining for 30 min at room temperature, cells were washed with 1× PBS, similar to the first panel. Samples were fixed with Life Technologies IC Fixation Buffer (FB001) from ThermoFisher Scientific (Waltham, Massachusetts, USA) according to the manufacturer's protocol and resuspended in FACS buffer.

To determine viability, all flow cytometry panels used LIVE/DEAD® Fixable Aqua Dead Cell Stain (L34957) from ThermoFisher Scientific. Samples were run in a BD Celesta Cell Analyzer, recording at least 30,000 events. The results were analyzed using FlowJo software 10.4.

Quantitative real-time PCR. SM1 murine melanoma cells were plated in a 6-well plate. Cells were serum starved overnight followed by pre-treatment with 5 μM SS-208 for 1 h. Subsequently, treatment with recombinant murine IL-6 (Biolegend, San Diego, CA 92121) at 30 ng/mL was performed for overnight. Following the manufacturer's instructions, Total RNA was extracted from cells using the Trizol (Life Technologies, Carlsbad, CA, 92008). Samples were processed immediately or stored at -80 °C. Quantification of RNA was done using a ND-1000 NanoDrop Spectrophotometer (NanoDrop Technologies, Inc., Wilmington, Delaware). The 260/280 ratios were routinely over 1.9. Sample cDNA was produced using the iScript cDNA synthesis kit (Bio-Rad, 1708891). Target mRNA was quantified using iQ SYBR green Supermix (Bio-Rad, 1708882). Primers targeting PD-L1 and GAPDH for qRT-PCR were purchased from Invitrogen (Waltham, Massachusetts, USA) and the sequences are listed in the previous publication.[51] Cycling conditions were used as per manufacturer's instructions. Single product amplification was confirmed by melting curve analysis, and primer efficiency was near 100% in all the experiments

performed. Quantification is expressed in arbitrary units, and target mRNA levels were normalized to GAPDH expression using the method described by Pfaffl et al[101] using Microsoft Excel Software (Microsoft, Redmond, WA).

Immunoblotting. Cells were lysed in RIPA buffer (Pierce, 89900) with 1× protease and phosphatase inhibitor (Pierce, A32961). Lysates were sonicated in a Bioruptor™ (Diagenode, Denville, NJ, USA) in a 4 °C water bath for 8 min (8 cycles of 30 s on, 30 s off). Protein concentration was determined using a Pierce BCA Protein Assay Kit (Thermo Fisher Scientific, 23225) according to the manufacturer's protocol. Samples were mixed with NuPAGE LDS 4× loading gel (NP0007) and NuPAGE 10× reducing agent (NP0009) then placed on a heating block at 100 °C. Next, samples were loaded onto 4-20% (BioRad, 4561093) or 10% gels (BioRad, 4561033) and transferred to LF PVDF (BioRad, 170-4274). Membranes were blocked with LI-COR Biosciences (Lincoln, Nebraska, USA) Odyssey Blocking Buffer (927-40100). Bands were detected using an Azure Biosystems (Dublin, California, USA) Imaging System c600. The antibodies used for immunoblotting included: PD-L1 (ProSci, 4059), PD-L2 (ProSci, 4063), total STAT3 (Cell Signal, 12640), phosphor-STAT3 (Y705) (Cell Signal, 9138), α-Tubulin (Cell Signaling, 3873), Ac-α-Tubulin (Cell Signaling, 3971), histone H3 (Cell Signaling 3638), Ac-histone H3 (Cell Signaling 9649S), and HDAC6 (Assay Biotech C0226). Bands were analyzed using ImageJ (NIH).

Statistical analysis and reproducibility. Experiments were done in triplicate unless otherwise noted. Analysis was done using unpaired *t*-tests with significance at $p < 0.05$ and the Kaplan-Meier survival curves using GraphPad Prism 7. All analyses of cell viability, apoptosis, and cytotoxicity were completed using Microsoft Excel Software (Microsoft,

Redmond, WA).

ASSOCIATED CONTENT

Supporting Information

The Supporting Information is available free of charge on the ACS Publications website at DOI:

Additional data on the Ames test and the hERG assay, crystallization data collection and refinement statistics, and physicochemical properties, ^{1}H NMR spectra, and ^{13}C NMR spectra for compounds **7a-d**, **11a-d**, and **20a-c**.

Molecular formula strings including screening data.

Accession Codes

Atomic coordinates and corresponding structure factors for the drHDAC6-CD2/SS-208 complex have been deposited at the Protein Data Bank as the 6ROK entry.

AUTHOR INFORMATION

Corresponding Author

*(A.P.K.) E-mail: akozikowski@starwisetrx.com. Phone: +1-773-793-5866.

*(A.V.) E-mail: avillagra@email.gwu.edu. Phone: +1-202-994-9547.

ORCID

Sida Shen: 0000-0002-0295-2545

Maurício T. Tavares: 0000-0002-4400-7787

Guiping Zhang: 0000-0001-9818-4773

Cyril Bařinka: 0000-0003-2751-3060

Alan P. Kozikowski: 0000-0003-4795-5368

Alejandro Villagra: 0000-0001-9346-8355

Present Addresses

†S.S.: Departments of Chemistry, Center for Molecular Innovation and Drug Discovery, and Center for Developmental Therapeutics, Northwestern University, Evanston, Illinois 60208, United States.

M.T.T.: Department of Chemistry, Scripps Research, Jupiter, Florida 33458, United States.

Author Contributions

‡S.S. and M.H. contributed equally to this paper.

A.V. and A.P.K. conceived the original idea, initiated the project, and oversaw all the chemical, biological and *in vivo* experimental designs and data analysis. S.S. designed and synthesized compounds, oversaw all the experimental design, analyzed data, and wrote the manuscript with assistance from the other authors. M.H., S.N., and T.K. designed and performed all biological and *in vivo* experimental designs, analyzed data, and contributed to the manuscript writing. J.P. crystallized the drHDAC6/SS-208 complex; K.U. solved, refined and analyzed the drHDAC6/SS-208 X-ray structure; C.B. determined IC_{50} values of HDAC isoforms, analyzed data, and contributed to manuscript writing. M.T.T. and G.Z assisted the scale-up work of SS-208 and assisted in the preparation of the manuscript. C.A.Z. designed and performed the cellular HDAC target engagement assay; M.B.R. oversaw the experimental design and data analyses of target engagement study and assisted in the preparation of the manuscript.

Notes

The authors declare no competing financial interest.

ACKNOWLEDGMENTS

Funded by NIH R21 CA184612-01 and Melanoma Research Foundation CDA Grant Award (A.V.); NIH R01NS079183, R43HD093464, and R41AG058283 (A.P.K.). Additionally, this work was in part supported by the CAS (RVO: 86652036), the Czech Science Foundation (15-19640S), and project BIOCEV (CZ.1.05/1.1.00/02.0109) from the ERDF (C.B.). We would like to acknowledge the important technical contributions and advice of Kimberlyn Acklin, MS, SCYM(ASCP), at The George Washington University Flow Cytometry Core Facility and Bethany Rentz, RVT, at The George Washington University Office of Animal Research. We thank Petra Baranova and Barbora Havlinova for excellent technical assistance and Lucia Motlova for helping with crystallization experiments. We also thank Dr. Werner Tueckmantel for proofreading the article and providing comments. We acknowledge the Helmholtz-Zentrum Berlin for the allocation of synchrotron radiation beamtime at the MX14.2 beamline and the support by the project CALIPSOplus (Grant Agreement 730872) from the EU Framework Programme for Research and Innovation HORIZON 2020.

ABBREVIATIONS

ADMET, absorption, distribution, metabolism, excretion, and toxicity; TPSA: topological polar surface area; MW: molecular weight; hERG: human Ether-à-go-go related gene; DEAD: diethyl azodicarboxylate; PCC: pyridinium chlorochromate; NCS: *N*-chlorosuccinimide; TFA: trifluoroacetic acid; DMF, *N*,*N*-dimethylformamide; DMSO, dimethyl sulfoxide; DCM, dichloromethane; DCE, 1,2-dichloroethane; THF, tetrahydrofuran; PD-L1/2: programmed death-ligand 1/2; PD-1: programmed cell death-1;

CTLA-4: cytotoxic T-lymphocyte-associated protein 4; MHC: major histocompatibility complex; CD25/40/80: Cluster of differentiation 25/40/80.

REFERENCES

1. Stone, A.; Cooper, J.; Koenig, K. L.; Golfinos, J. G.; Oratz, R. A comparison of survival rates for treatment of melanoma metastatic to the brain. *Cancer Invest.* **2004**, *22*, 492-497.

2. Miranda, E. P. Management of cutaneous melanoma. *N. Engl. J. Med.* **2004**, *351*, 2770-2771; author reply 2770-2771.

3. Luke, J. J.; Flaherty, K. T.; Ribas, A.; Long, G. V. Targeted agents and immunotherapies: optimizing outcomes in melanoma. *Nat. Rev. Clin. Oncol.* **2017**, *14*, 463-482.

4. Livingstone, E.; Zimmer, L.; Vaubel, J.; Schadendorf, D. BRAF, MEK and KIT inhibitors for melanoma: adverse events and their management. *Chin. Clin. Oncol.* **2014**, *3*, 29.

5. Waterhouse, P.; Penninger, J. M.; Timms, E.; Wakeham, A.; Shahinian, A.; Lee, K. P.; Thompson, C. B.; Griesser, H.; Mak, T. W. Lymphoproliferative disorders with early lethality in mice deficient in Ctla-4. *Science* **1995,** *270*, 985-988.

6. Polkowska, M.; Ekk-Cierniakowski, P.; Czepielewska, E.; Kozlowska-Wojciechowska, M. Efficacy and safety of BRAF inhibitors and anti-CTLA4 antibody in melanoma patients-real-world data. *Eur. J. Clin. Pharmacol.* **2018**, *75*, 329-334.

7. Robert, C.; Schachter, J.; Long, G. V.; Arance, A.; Grob, J. J.; Mortier, L.; Daud, A.; Carlino, M. S.; McNeil, C.; Lotem, M.; Larkin, J.; Lorigan, P.; Neyns, B.; Blank, C. U.; Hamid, O.; Mateus, C.; Shapira-Frommer, R.; Kosh, M.; Zhou, H.; Ibrahim, N.; Ebbinghaus, S.; Ribas, A.; Keynote-006 investigators. Pembrolizumab versus ipilimumab

in advanced melanoma. *N. Engl. J. Med.* **2015**, *372*, 2521-2532.

8. Weber, J.; Mandala, M.; Del Vecchio, M.; Gogas, H. J.; Arance, A. M.; Cowey, C. L.; Dalle, S.; Schenker, M.; Chiarion-Sileni, V.; Marquez-Rodas, I.; Grob, J. J.; Butler, M. O.; Middleton, M. R.; Maio, M.; Atkinson, V.; Queirolo, P.; Gonzalez, R.; Kudchadkar, R. R.; Smylie, M.; Meyer, N.; Mortier, L.; Atkins, M. B.; Long, G. V.; Bhatia, S.; Lebbe, C.; Rutkowski, P.; Yokota, K.; Yamazaki, N.; Kim, T. M.; de Pril, V.; Sabater, J.; Qureshi, A.; Larkin, J.; Ascierto, P. A.; CheckMate 238 Collaborators. Adjuvant nivolumab versus ipilimumab in resected stage III or IV melanoma. *N. Engl. J. Med.* **2017**, *377*, 1824-1835.

9. Wolchok, J. D.; Chiarion-Sileni, V.; Gonzalez, R.; Rutkowski, P.; Grob, J. J.; Cowey, C. L.; Lao, C. D.; Wagstaff, J.; Schadendorf, D.; Ferrucci, P. F.; Smylie, M.; Dummer, R.; Hill, A.; Hogg, D.; Haanen, J.; Carlino, M. S.; Bechter, O.; Maio, M.; Marquez-Rodas, I.; Guidoboni, M.; McArthur, G.; Lebbe, C.; Ascierto, P. A.; Long, G. V.; Cebon, J.; Sosman, J.; Postow, M. A.; Callahan, M. K.; Walker, D.; Rollin, L.; Bhore, R.; Hodi, F. S.; Larkin, J. Overall survival with combined nivolumab and ipilimumab in advanced melanoma. *N. Engl. J. Med.* **2017**, *377*, 1345-1356.

10. O'Sullivan Coyne, G.; Madan, R. A.; Gulley, J. L. Nivolumab: promising survival signal coupled with limited toxicity raises expectations. *J. Clin. Oncol.* **2014**, *32*, 986-988.

11. O'Donnell, J. S.; Smyth, M. J.; Teng, M. W. Acquired resistance to anti-PD1 therapy: checkmate to checkpoint blockade? *Genome Med.* **2016**, *8*, 111.

12. Gide, T. N.; Wilmott, J. S.; Scolyer, R. A.; Long, G. V. Primary and acquired resistance to immune checkpoint inhibitors in metastatic melanoma. *Clin. Cancer. Res.* **2018**, *24*, 1260-1270.

13. Datta, M.; Coussens, L. M.; Nishikawa, H.; Hodi, F. S.; Jain, R. K. Reprogramming

the tumor microenvironment to improve immunotherapy: emerging strategies and combination therapies. *Am. Soc. Clin. Oncol. Educ. Book* **2019**, 165-174.

14. Kowal, J.; Kornete, M.; Joyce, J. A. Re-education of macrophages as a therapeutic strategy in cancer. *Immunotherapy* **2019**, *11*, 677-689.

15. Voorwerk, L.; Slagter, M.; Horlings, H. M.; Sikorska, K.; van de Vijver, K. K.; de Maaker, M.; Nederlof, I.; Kluin, R. J. C.; Warren, S.; Ong, S.; Wiersma, T. G.; Russell, N. S.; Lalezari, F.; Schouten, P. C.; Bakker, N. A. M.; Ketelaars, S. L. C.; Peters, D.; Lange, C. A. H.; van Werkhoven, E.; van Tinteren, H.; Mandjes, I. A. M.; Kemper, I.; Onderwater, S.; Chalabi, M.; Wilgenhof, S.; Haanen, J.; Salgado, R.; de Visser, K. E.; Sonke, G. S.; Wessels, L. F. A.; Linn, S. C.; Schumacher, T. N.; Blank, C. U.; Kok, M. Immune induction strategies in metastatic triple-negative breast cancer to enhance the sensitivity to PD-1 blockade: the TONIC trial. *Nat. Med.* **2019**, *25*, 920-928.

16. Choi, J.; Gyamfi, J.; Jang, H.; Koo, J. S. The role of tumor-associated macrophage in breast cancer biology. *Histol. Histopathol.* **2018**, *33*, 133-145.

17. Kim, H. J.; Bae, S. C. Histone deacetylase inhibitors: molecular mechanisms of action and clinical trials as anti-cancer drugs. *Am. J. Transl. Res.* **2011**, *3*, 166-179.

18. Li, T.; Zhang, C.; Hassan, S.; Liu, X.; Song, F.; Chen, K.; Zhang, W.; Yang, J. Histone deacetylase 6 in cancer. *J. Hematol. Oncol.* **2018**, *11*, 111.

19. Ganai, S. A. Histone deacetylase inhibitors modulating non-epigenetic players: the novel mechanism for small molecule based therapeutic intervention. *Curr. Drug Targets* **2018**, *19*, 593-601.

20. Glozak, M. A.; Sengupta, N.; Zhang, X.; Seto, E. Acetylation and deacetylation of non-histone proteins. *Gene* **2005**, *363*, 15-23.

21. Li, Y.; Seto, E. HDACs and HDAC inhibitors in cancer development and therapy. *Cold Spring Harb. Perspect Med.* **2016,** *6*, a026831..

22. Eckschlager, T.; Plch, J.; Stiborova, M.; Hrabeta, J. Histone deacetylase inhibitors as anticancer drugs. *Int. J. Mol. Sci.* **2017**, *18*, E1414.

23. Landreville, S.; Agapova, O. A.; Matatall, K. A.; Kneass, Z. T.; Onken, M. D.; Lee, R. S.; Bowcock, A. M.; Harbour, J. W. Histone deacetylase inhibitors induce growth arrest and differentiation in uveal melanoma. *Clin. Cancer Res.* **2012**, *18*, 408-416.

24. Clawson, G. A. Histone deacetylase inhibitors as cancer therapeutics. *Ann. Transl. Med.* **2016**, *4*, 287.

25. Shen, L.; Orillion, A.; Pili, R. Histone deacetylase inhibitors as immunomodulators in cancer therapeutics. *Epigenomics* **2016**, *8*, 415-428.

26. Hornig, E.; Heppt, M. V.; Graf, S. A.; Ruzicka, T.; Berking, C. Inhibition of histone deacetylases in melanoma-a perspective from bench to bedside. *Exp. Dermatol.* **2016**, *25*, 831-838.

27. Woods, D. M.; Sodre, A. L.; Villagra, A.; Sarnaik, A.; Sotomayor, E. M.; Weber, J. HDAC inhibition upregulates PD-1 ligands in melanoma and augments immunotherapy with PD-1 blockade. *Cancer Immunol. Res.* **2015**, *3*, 1375-1385.

28. Woan, K. V.; Lienlaf, M.; Perez-Villaroel, P.; Lee, C.; Cheng, F.; Knox, T.; Woods, D. M.; Barrios, K.; Powers, J.; Sahakian, E.; Wang, H. W.; Canales, J.; Marante, D.; Smalley, K. S. M.; Bergman, J.; Seto, E.; Kozikowski, A.; Pinilla-Ibarz, J.; Sarnaik, A.; Celis, E.; Weber, J.; Sotomayor, E. M.; Villagra, A. Targeting histone deacetylase 6 mediates a dual anti-melanoma effect: enhanced antitumor immunity and impaired cell proliferation. *Mol. Oncol.* **2015**, *9*, 1447-1457.

29. Roche, J.; Bertrand, P. Inside HDACs with more selective HDAC inhibitors. *Eur. J. Med. Chem.* **2016**, *121*, 451-483.

30. Guerriero, J. L.; Sotayo, A.; Ponichtera, H. E.; Castrillon, J. A.; Pourzia, A. L.; Schad, S.; Johnson, S. F.; Carrasco, R. D.; Lazo, S.; Bronson, R. T.; Davis, S. P.; Lobera, M.; Nolan, M. A.; Letai, A. Class IIa HDAC inhibition reduces breast tumours and metastases through anti-tumour macrophages. *Nature* **2017**, *543*, 428-432.

31. Lee, J. H.; Yao, Y.; Mahendran, A.; Ngo, L.; Venta-Perez, G.; Choy, M. L.; Breslow, R.; Marks, P. A. Creation of a histone deacetylase 6 inhibitor and its biological effects [corrected]. *Proc. Natl. Acad. Sci. U. S. A.* **2015**, *112*, 12005-12010.

32. Hsieh, H. Y.; Chuang, H. C.; Shen, F. H.; Detroja, K.; Hsin, L. W.; Chen, C. S. Targeting breast cancer stem cells by novel HDAC3-selective inhibitors. *Eur. J. Med. Chem.* **2017**, *140*, 42-51.

33. Hideshima, T.; Mazitschek, R.; Qi, J.; Mimura, N.; Tseng, J. C.; Kung, A. L.; Bradner, J. E.; Anderson, K. C. HDAC6 inhibitor WT161 downregulates growth factor receptors in breast cancer. *Oncotarget* **2017**, *8*, 80109-80123.

34. Lee, H. Y.; Nepali, K.; Huang, F. I.; Chang, C. Y.; Lai, M. J.; Li, Y. H.; Huang, H. L.; Yang, C. R.; Liou, J. P. (*N*-Hydroxycarbonylbenylamino)quinolines as selective histone deacetylase 6 inhibitors suppress growth of multiple myeloma in vitro and in vivo. *J. Med. Chem.* **2018**, *61*, 905-917.

35. Tavares, M. T.; Shen, S.; Knox, T.; Hadley, M.; Kutil, Z.; Barinka, C.; Villagra, A.; Kozikowski, A. P. Synthesis and pharmacological evaluation of selective histone deacetylase 6 inhibitors in melanoma models. *ACS Med. Chem. Lett.* **2017**, *8*, 1031-1036.

36. de Ruijter, A. J.; van Gennip, A. H.; Caron, H. N.; Kemp, S.; van Kuilenburg, A. B.

Histone deacetylases (HDACs): characterization of the classical HDAC family. *Biochem. J.* **2003**, *370*, 737-749.

37. Haberland, M.; Montgomery, R. L.; Olson, E. N. The many roles of histone deacetylases in development and physiology: implications for disease and therapy. *Nat. Rev. Genet.* **2009**, *10*, 32-42.

38. Matthias, P.; Yoshida, M.; Khochbin, S. HDAC6 a new cellular stress surveillance factor. *Cell Cycle* **2008**, *7*, 7-10.

39. Imai, Y.; Maru, Y.; Tanaka, J. Action mechanisms of histone deacetylase inhibitors in the treatment of hematological malignancies. *Cancer Sci.* **2016**, *107*, 1543-1549.

40. Miyake, Y.; Keusch, J. J.; Wang, L.; Saito, M.; Hess, D.; Wang, X.; Melancon, B. J.; Helquist, P.; Gut, H.; Matthias, P. Structural insights into HDAC6 tubulin deacetylation and its selective inhibition. *Nat. Chem. Biol.* **2016**, *12*, 748-754.

41. Faria Freitas, M.; Cuendet, M.; Bertrand, P. HDAC inhibitors: a 2013-2017 patent survey. *Expert Opin. Ther. Pat.* **2018**, 1-17.

42. Clinical trials for ACY-1215. <https://clinicaltrials.gov/ct2/results?term=ACY-1215&Search=Search>. Accessed Mar. 15, 2019.

43. Clinical trials for ACY-241. <https://clinicaltrials.gov/ct2/results?term=ACY-241&Search=Search>. Accessed Mar. 15, 2019.

44. Fukada, M.; Hanai, A.; Nakayama, A.; Suzuki, T.; Miyata, N.; Rodriguiz, R. M.; Wetsel, W. C.; Yao, T. P.; Kawaguchi, Y. Loss of deacetylation activity of Hdac6 affects emotional behavior in mice. *PLoS One* **2012**, *7*, e30924.

45. Jochems, J.; Boulden, J.; Lee, B. G.; Blendy, J. A.; Jarpe, M.; Mazitschek, R.; Van Duzer, J. H.; Jones, S.; Berton, O. Antidepressant-like properties of novel HDAC6-

selective inhibitors with improved brain bioavailability. *Neuropsychopharmacology* **2014**, *39*, 389-400.

46. d'Ydewalle, C.; Krishnan, J.; Chiheb, D. M.; Van Damme, P.; Irobi, J.; Kozikowski, A. P.; Vanden Berghe, P.; Timmerman, V.; Robberecht, W.; Van Den Bosch, L. HDAC6 inhibitors reverse axonal loss in a mouse model of mutant HSPB1-induced Charcot-Marie-Tooth disease. *Nat. Med.* **2011**, *17*, 968-974.

47. Liu, J.; Gu, J.; Feng, Z.; Yang, Y.; Zhu, N.; Lu, W.; Qi, F. Both HDAC5 and HDAC6 are required for the proliferation and metastasis of melanoma cells. *J. Transl. Med.* **2016**, *14*, 7.

48. Liu, J.; Luan, W.; Zhang, Y.; Gu, J.; Shi, Y.; Yang, Y.; Feng, Z.; Qi, F. HDAC6 interacts with PTPN1 to enhance melanoma cells progression. *Biochem. Biophys. Res. Commun.* **2018**, *495*, 2630-2636.

49. Peng, U.; Wang, Z.; Pei, S.; Ou, Y.; Hu, P.; Liu, W.; Song, J. ACY-1215 accelerates vemurafenib induced cell death of BRAF-mutant melanoma cells via induction of ER stress and inhibition of ERK activation. *Oncol. Rep.* **2017**, *37*, 1270-1276.

50. Lienlaf, M.; Perez-Villarroel, P.; Knox, T.; Pabon, M.; Sahakian, E.; Powers, J.; Woan, K.V.; Lee, C.; Cheng, F.; Deng, S.; Smalley, K. S. M.; Montecino, M.; Kozikowski, A.; Pinilla-Ibarz, J.; Sarnaik, A.; Seto, E.; Weber, J.; Sotomayor, E. M.; Villagra, A. Essential role of HDAC6 in the regulation of PD-L1 in melanoma. *Mol. Oncol.* **2016**, *10*, 735-750.

51. Knox, T.; Sahakian, E.; Banik, D.; Hadley, M.; Palmer, E.; Noonepalle, S.; Kim, J.; Powers, J.; Gracia-Hernandez, M.; Oliveira, V.; Cheng, F.; Chen, J.; Barinka, C.; Pinilla-Ibarz, J.; Lee, N. H.; Kozikowski, A.; Villagra, A. Selective HDAC6 inhibitors improve anti-PD-1 immune checkpoint blockade therapy by decreasing the anti-inflammatory

phenotype of macrophages and down-regulation of immunosuppressive proteins in tumor cells. *Sci. Rep.* **2019**, *9*, 6136.

52. Huang, P.; Almeciga-Pinto, I.; Jarpe, M.; van Duzer, J. H.; Mazitschek, R.; Yang, M.; Jones, S. S.; Quayle, S. N. Selective HDAC inhibition by ACY-241 enhances the activity of paclitaxel in solid tumor models. *Oncotarget* **2017**, *8*, 2694-2707.

53. Santo, L.; Hideshima, T.; Kung, A. L.; Tseng, J. C.; Tamang, D.; Yang, M.; Jarpe, M.; van Duzer, J. H.; Mazitschek, R.; Ogier, W. C.; Cirstea, D.; Rodig, S.; Eda, H.; Scullen, T.; Canavese, M.; Bradner, J.; Anderson, K. C.; Jones, S. S.; Raje, N. Preclinical activity, pharmacodynamic, and pharmacokinetic properties of a selective HDAC6 inhibitor, ACY-1215, in combination with bortezomib in multiple myeloma. *Blood* **2012**, *119*, 2579-2589.

54. Zhang, Y.; Ying, J. B.; Hong, J. J.; Li, F. C.; Fu, T. T.; Yang, F. Y.; Zheng, G. X.; Yao, X. J.; Lou, Y.; Qiu, Y.; Xue, W. W.; Zhu, F. How does chirality determine the selective inhibition of histone deacetylase 6? A lesson from trichostatin A enantiomers based on molecular dynamics. *ACS Chem. Neurosci.* **2019**, *10*, 2467-2480.

55. Butler, K. V.; Kalin, J.; Brochier, C.; Vistoli, G.; Langley, B.; Kozikowski, A. P. Rational design and simple chemistry yield a superior, neuroprotective HDAC6 inhibitor, tubastatin A. *J. Am. Chem. Soc.* **2010**, *132*, 10842-10846.

56. Bergman, J. A.; Woan, K.; Perez-Villarroel, P.; Villagra, A.; Sotomayor, E. M.; Kozikowski, A. P. Selective histone deacetylase 6 inhibitors bearing substituted urea linkers inhibit melanoma cell growth. *J. Med. Chem.* **2012**, *55*, 9891-9899.

57. Strebl, M. G.; Campbell, A. J.; Zhao, W. N.; Schroeder, F. A.; Riley, M. M.; Chindavong, P. S.; Morin, T. M.; Haggarty, S. J.; Wagner, F. F.; Ritter, T.; Hooker, J. M. HDAC6 brain mapping with [(18)F]Bavarostat enabled by a Ru-mediated

deoxyfluorination. *ACS Cent. Sci.* **2017**, *3*, 1006-1014.

58. De Vreese, R.; Van Steen, N.; Verhaeghe, T.; Desmet, T.; Bougarne, N.; De Bosscher, K.; Benoy, V.; Haeck, W.; Van Den Bosch, L.; D'Hooghe, M. Synthesis of benzothiophene-based hydroxamic acids as potent and selective HDAC6 inhibitors. *Chem. Commun.* **2015**, *51*, 9868-9871.

59. Shen, S.; Benoy, V.; Bergman, J. A.; Kalin, J. H.; Frojuello, M.; Vistoli, G.; Haeck, W.; Van Den Bosch, L.; Kozikowski, A. P. Bicyclic-capped histone deacetylase 6 inhibitors with improved activity in a model of axonal Charcot-Marie-Tooth disease. *ACS Chem. Neurosci.* **2016**, *7*, 240-258.

60. Lee, H. Y.; Fan, S. J.; Huang, F. I.; Chao, H. Y.; Hsu, K. C.; Lin, T. E.; Yeh, T. K.; Lai, M. J.; Li, Y. H.; Huang, H. L.; Yang, C. R.; Liou, J. P. 5-Aroylindoles act as selective histone deacetylase 6 inhibitors ameliorating Alzheimer's disease phenotypes. *J. Med. Chem.* **2018**, *61*, 7087-7102.

61. De Vreese, R.; Galle, L.; Depetter, Y.; Franceus, J.; Desmet, T.; Van Hecke, K.; Benoy, V.; Van Den Bosch, L.; D'Hooghe, M. Synthesis of potent and selective HDAC6 inhibitors bearing a cyclohexane- or cycloheptane-annulated 1,5-benzothiazepine scaffold. *Chemistry* **2017**, *23*, 128-136.

62. De Vreese, R.; Depetter, Y.; Verhaeghe, T.; Desmet, T.; Benoy, V.; Haeck, W.; Van Den Bosch, L.; D'Hooghe, M. Synthesis and SAR assessment of novel Tubathian analogs in the pursuit of potent and selective HDAC6 inhibitors. *Org. Biomol. Chem.* **2016**, *14*, 2537-2549.

63. Kozikowski, A.; Shen, S.; Pardo, M.; Tavares, M. T.; Szarics, D.; Benoy, V.; Zimprich, C. A.; Kutil, Z.; Zhang, G.; Barinka, C.; Robers, M. B.; Van Den Bosch, L.; Eubanks, J.

H.; Jope, R. S. Brain penetrable histone deacetylase 6 inhibitor SW-100 ameliorates memory and learning impairments in a mouse model of Fragile X Syndrome. *ACS Chem. Neurosci.* **2018**, *10*, 1679-1695.

64. Vogerl, K.; Ong, N.; Senger, J.; Herp, D.; Schmidtkunz, K.; Marek, M.; Muller, M.; Bartel, K.; Shaik, T. B.; Porter, N. J.; Robaa, D.; Christianson, D. W.; Romier, C.; Sippl, W.; Jung, M.; Bracher, F. Synthesis and biological investigation of phenothiazine-based benzhydroxamic acids as selective histone deacetylase 6 inhibitors. *J. Med. Chem.* **2019**, *62*, 1138-1166.

65. Wang, X. X.; Wan, R. Z.; Liu, Z. P. Recent advances in the discovery of potent and selective HDAC6 inhibitors. *Eur. J. Med. Chem.* **2018**, *143*, 1406-1418.

66. De Vreese, R.; D'Hooghe, M. Synthesis and applications of benzohydroxamic acid-based histone deacetylase inhibitors. *Eur. J. Med. Chem.* **2017**, *135*, 174-195.

67. Schlimme, S.; Hauser, A. T.; Carafa, V.; Heinke, R.; Kannan, S.; Stolfa, D. A.; Cellamare, S.; Carotti, A.; Altucci, L.; Jung, M.; Sippl, W. Carbamate prodrug concept for hydroxamate HDAC inhibitors. *ChemMedChem* **2011**, *6*, 1193-1198.

68. Senger, J.; Melesina, J.; Marek, M.; Romier, C.; Oehme, I.; Witt, O.; Sippl, W.; Jung, M. Synthesis and biological investigation of oxazole hydroxamates as highly selective histone deacetylase 6 (HDAC6) inhibitors. *J. Med. Chem.* **2016**, *59*, 1545-1555.

69. Zhu, J.; Mo, J.; Lin, H. Z.; Chen, Y.; Sun, H. P. The recent progress of isoxazole in medicinal chemistry. *Bioorg. Med. Chem.* **2018**, *26*, 3065-3075.

70. Sysak, A.; Obminska-Mrukowicz, B. Isoxazole ring as a useful scaffold in a search for new therapeutic agents. *Eur. J. Med. Chem.* **2017**, *137*, 292-309.

71. Gaisina, I. N.; Tueckmantel, W.; Ugolkov, A.; Shen, S.; Hoffen, J.; Dubrovskyi, O.;

Mazar, A.; Schoon, R. A.; Billadeau, D.; Kozikowski, A. P. Identification of HDAC6-selective inhibitors of low cancer cell cytotoxicity. *ChemMedChem* **2016**, *11*, 81-92.

72. Kozikowski, A. P.; Tapadar, S.; Luchini, D. N.; Kim, K. H.; Billadeau, D. D. Use of the nitrile oxide cycloaddition (NOC) reaction for molecular probe generation: a new class of enzyme selective histone deacetylase inhibitors (HDACIs) showing picomolar activity at HDAC6. *J. Med. Chem.* **2008**, *51*, 4370-4373.

73. Tapadar, S.; He, R.; Luchini, D. N.; Billadeau, D. D.; Kozikowski, A. P. Isoxazole moiety in the linker region of HDAC inhibitors adjacent to the Zn-chelating group: effects on HDAC biology and antiproliferative activity. *Bioorg. Med. Chem. Lett.* **2009**, *19*, 3023-3026.

74. Daina, A.; Michielin, O.; Zoete, V. SwissADME: a free web tool to evaluate pharmacokinetics, drug-likeness and medicinal chemistry friendliness of small molecules. *Sci. Rep.* **2017**, *7*, 42717.

75. Shen, S.; Kozikowski, A. P. Why hydroxamates may not be the best histone deacetylase inhibitors--What some may have forgotten or would rather forget? *ChemMedChem* **2016**, *11*, 15-21.

76. Simoni, D.; Invidiata, F. P.; Rondanin, R.; Grimaudo, S.; Cannizzo, G.; Barbusca, E.; Porretto, F.; D'Alessandro, N.; Tolomeo, M. Structure-activity relationship studies of novel heteroretinoids: induction of apoptosis in the HL-60 cell line by a novel isoxazole-containing heteroretinoid. *J. Med. Chem.* **1999**, *42*, 4961-4969.

77. Segretti, M. C.; Vallerini, G. P.; Brochier, C.; Langley, B.; Wang, L.; Hancock, W. W.; Kozikowski, A. P. Thiol-based potent and selective HDAC6 inhibitors promote tubulin acetylation and T-regulatory cell suppressive function. *ACS Med. Chem. Lett.* **2015**, *6*,

1156-1161.

78. Lv, W.; Zhang, G.; Barinka, C.; Eubanks, J. H.; Kozikowski, A. P. Design and synthesis of mercaptoacetamides as potent, selective, and brain permeable histone deacetylase 6 inhibitors. *ACS Med Chem Lett* **2017,** *8*, 510-515.

79. Parmenon, C.; Guillard, J.; Caignard, D. H.; Hennuyer, N.; Staels, B.; Audinot-Bouchez, V.; Boutin, J. A.; Dacquet, C.; Ktorza, A.; Viaud-Massuard, M. C. 4,4-Dimethyl-1,2,3,4-tetrahydroquinoline-based PPARalpha/gamma agonists. Part I: synthesis and pharmacological evaluation. *Bioorg. Med. Chem. Lett.* **2008**, *18*, 1617-1622.

80. Elliott, E. C.; Regan, S. L.; Maggs, J. L.; Bowkett, E. R.; Parry, L. J.; Williams, D. P.; Park, B. K.; Stachulski, A. V. Haloarene derivatives of carbamazepine with reduced bioactivation liabilities: 2-monohalo and 2,8-dihalo derivatives. *J. Med. Chem.* **2012**, *55*, 9773-9784.

81. Martinez-Asencio, A.; Yus, M.; Ramon, D. J. Copper(II) acetate-catalyzed one-pot conversion of aldehydes into primary amides through a Beckmann-type rearrangement. *Tetrahedron* **2012**, *68*, 3948-3951.

82. Dube, D.; Scholte, A. A. Reductive N-alkylation of amides, carbamates and ureas. *Tetrahedron Lett.* **1999**, *40*, 2295-2298.

83. Hopkins, A. L.; Groom, C. R.; Alex, A. Ligand efficiency: a useful metric for lead selection. *Drug Discov. Today* **2004**, *9*, 430-431.

84. Johnson, T. W.; Gallego, R. A.; Edwards, M. P. Lipophilic efficiency as an important metric in drug design. *J. Med. Chem.* **2018**, *61*, 6401-6420.

85. Porter, N. J.; Mahendran, A.; Breslow, R.; Christianson, D. W. Unusual zinc-binding mode of HDAC6-selective hydroxamate inhibitors. *Proc. Natl. Acad. Sci. U. S. A.* **2017**,

114, 13459-13464.

86. Porter, N. J.; Wagner, F. F.; Christianson, D. W. Entropy as a driver of selectivity for inhibitor binding to histone deacetylase 6. *Biochemistry* **2018**, *57*, 3916-3924.

87. Porter, N. J.; Osko, J. D.; Diedrich, D.; Kurz, T.; Hooker, J. M.; Hansen, F. K.; Christianson, D. W. Histone deacetylase 6-selective inhibitors and the influence of capping groups on hydroxamate-zinc denticity. *J. Med. Chem.* **2018**, *61*, 8054-8060.

88. Hai, Y.; Christianson, D. W. Histone deacetylase 6 structure and molecular basis of catalysis and inhibition. *Nat. Chem. Biol.* **2016**, *12*, 741-747.

89. Robers, M. B.; Dart, M. L.; Woodroofe, C. C.; Zimprich, C. A.; Kirkland, T. A.; Machleidt, T.; Kupcho, K. R.; Levin, S.; Hartnett, J. R.; Zimmerman, K.; Niles, A. L.; Ohana, R. F.; Daniels, D. L.; Slater, M.; Wood, M. G.; Cong, M.; Cheng, Y. Q.; Wood, K. V. Target engagement and drug residence time can be observed in living cells with BRET. *Nat. Commun.* **2015**, *6*, 10091.

90. Mills, C. D.; Lenz, L. L.; Harris, R. A. A Breakthrough: macrophage-directed cancer immunotherapy. *Cancer Res.* **2016**, *76*, 513-516.

91. Yang, L.; Zhang, Y. Tumor-associated macrophages: from basic research to clinical application. *J. Hematol. Oncol.* **2017**, *10*, 58.

92. Skultetyova, L.; Ustinova, K.; Kutil, Z.; Novakova, Z.; Pavlicek, J.; Mikesova, J.; Trapl, D.; Baranova, P.; Havlinova, B.; Hubalek, M.; Lansky, Z.; Barinka, C. Human histone deacetylase 6 shows strong preference for tubulin dimers over assembled microtubules. *Sci. Rep.* **2017**, *7*, 11547.

93. Kutil, Z.; Novakova, Z.; Meleshin, M.; Mikesova, J.; Schutkowski, M.; Barinka, C. Histone deacetylase 11 is a fatty-acid deacylase. *ACS Chem. Biol.* **2018**, *13*, 685-693.

94. Wu, H.; Yang, K.; Zhang, Z.; Leisten, E.; Li, Z.; Xie, H.; Liu, J.; Smith, K. A.; Novakova, Z.; Barinka, C.; Tang, W., Development of multi-functional histone deacetylase 6 degraders with potent anti-myeloma activity. *J Med Chem* **2019**. doi: 10.1021/acs.jmedchem.9b00516.

95. Sparta, K. M.; Krug, M.; Heinemann, U.; Mueller, U.; Weiss, M. S. Xdsapp2.0. *J. Appl. Crystallogr.* **2016**, *49*, 1085-1092.

96. Vagin, A. A.; Steiner, R. A.; Lebedev, A. A.; Potterton, L.; McNicholas, S.; Long, F.; Murshudov, G. N. REFMAC5 dictionary: organization of prior chemical knowledge and guidelines for its use. *Acta Crystallogr. D* **2004**, *60*, 2184-2195.

97. Emsley, P.; Lohkamp, B.; Scott, W. G.; Cowtan, K. Features and development of Coot. *Acta Crystallogr. D* **2010**, *66*, 486-501.

98. Long, F.; Nicholls, R. A.; Emsley, P.; Grazulis, S.; Merkys, A.; Vaitkus, A.; Murshudov, G. N. AceDRG: a stereochemical description generator for ligands. *Acta Crystallogr. D* **2017**, *73*, 112-122.

99. Chen, V. B.; Arendall, W. B.; Headd, J. J.; Keedy, D. A.; Immormino, R. M.; Kapral, G. J.; Murray, L. W.; Richardson, J. S.; Richardson, D. C. MolProbity: all-atom structure validation for macromolecular crystallography. *Acta Crystallogr. D* **2010**, *66*, 12-21.

100. Koya, R. C.; Mok, S.; Otte, N.; Blacketor, K. J.; Comin-Anduix, B.; Tumeh, P. C.; Minasyan, A.; Graham, N. A.; Graeber, T. G.; Chodon, T.; Ribas, A. BRAF inhibitor vemurafenib improves the antitumor activity of adoptive cell immunotherapy. *Cancer Res.* **2012**, *72*, 3928-37.

101. Pfaffl, M. W. A new mathematical model for relative quantification in real-time RT-PCR. *Nucleic Acids Res.* **2001**, *29*, e45.

Table of Contents graphic

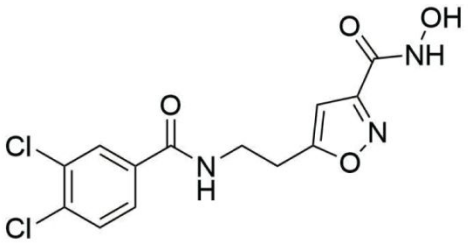

SS-208

HDAC6 (IC_{50}) = 12 nM HDAC7 (IC_{50}) = 8340 nM
HDAC1 (IC_{50}) = 1390 nM HDAC8 (IC_{50}) = 1230 nM
HDAC4 (IC_{50}) = 19500 nM HDAC9 (IC_{50}) = 38200 nM
HDAC5 (IC_{50}) = 6910 nM HDAC11 (IC_{50}) = 5120 nM